Biochimica et Biophysica Acta 1838 (2014) 1031–1046

Contents lists available at ScienceDirect

Biochimica et Biophysica Acta

journal homepage: www.elsevier.com/locate/bbamem

Insights into the molecular basis of action of the AT_1 antagonist losartan using a combined NMR spectroscopy and computational approach

Maria Zervou [a,*], Zoe Cournia [b], Constantinos Potamitis [a], George Patargias [b], Serdar Durdagi [a,1], Simona Golic Grdadolnik [c,d], Thomas Mavromoustakos [a,e]

[a] National Hellenic Research Foundation, Institute of Biology, Medicinal Chemistry & Biotechnology, Vas. Constantinou 48, 11635 Athens, Greece
[b] Biomedical Research Foundation of the Academy of Athens, 4, Soranou Efesiou, 11527 Athens, Greece
[c] Laboratory of Biomolecular Structure, National Institute of Chemistry, Hajdrihova 19, POB 30, SI-1115 Ljubljana, Slovenia
[d] EN-FIST Centre of Excellence, Dunajska 156, SI-1000 Ljubljana, Slovenia
[e] Chemistry Department of National Capodistrian University, Zographou, Athens 15784, Greece

ARTICLE INFO

Article history:
Received 12 August 2013
Received in revised form 17 December 2013
Accepted 19 December 2013
Available online 27 December 2013

Keywords:
Losartan
SDS micelles
NMR (DOSY, NOESY/ROESY)
Spin labels
Molecular dynamics in micelles
Molecular dynamics in phospholipid bilayers with embedded AT_1 receptor

ABSTRACT

The drug:membrane interactions for the antihypertensive AT1 antagonist losartan, the prototype of the sartans class, are studied herein using an integrated approach. The pharmacophore arrangement of the drug was revealed by rotating frame nuclear Overhauser effect spectroscopy (2D ROESY) NMR spectroscopy in three different environments, namely water, dimethyl sulfoxide (DMSO), and sodium dodecyl sulfate (SDS) micellar solutions mimicking conditions of biological transport fluids and membrane lipid bilayers. Drug association with micelles was monitored by diffusion ordered spectroscopy (2D DOSY) and drug:micelle intermolecular interactions were characterized by ROESY spectroscopy. The localisation of the drug in the micellar environment was investigated by introducing 5-doxyl and 16-doxyl stearic acids. The use of spin labels confirmed that losartan resides close to the micelle:water interface with the hydroxymethyl group and the tetrazole heterocyclic aromatic ring facing the polar surface with the potential to interact with SDS charged polar head groups in order to increase amphiphilic interactions. The spontaneous insertion, the diffusion pathway and the conformational features of losartan were monitored by Molecular Dynamics (MD) simulations in a modeled SDS micellar aggregate environment and a long exploratory MD run (580 ns) in a phospholipid dipalmitoylphosphatidylcholine (DPPC) bilayer with the AT_1 receptor embedded. MD simulations were in excellent agreement with experimental results and further revealed the molecular basis of losartan:membrane interactions in atomic-level detail. This applied integrated approach aims to explore the role of membranes in losartan's pathway towards the AT_1 receptor.

1. Introduction

In the absence of crystallographic or spectroscopic data associated with a specific target receptor such as in the case of the AT_1 receptor, which belongs to the class A G-protein-coupled receptors (GPCRs), a ligand-based pharmacophore approach or a model receptor using a solved structure as template from the same receptor class can be applied in virtual screening, *de novo* drug design, and lead optimization [1,2]. In the drug design process, one important aspect is the relationship between conformation and bioactivity [3,4]. Flexible pharmacophore segments of the ligand allow the drug to adopt different low-energy conformations comprising the bioactive conformation(s) upon binding in the active site of the target. Treating ligand conformational flexibility, is a challenging task for the process of alignment and the construction of pharmacophore models [1]. Tracing an ensemble of low energy drug conformers using NMR experimental restraints and conformational analysis methods could significantly assist the procedure.

Sartans are pharmaceuticals, which modulate the renin–angiotensin–aldosterone system. They antagonize with high selectivity the binding of the vasoconstrictor hormone Angiotensin II (ANG II) at the AT_1 receptor. Losartan potassium is a paradigm of successful rational drug design since its molecular structure is based on the mimicry of the C-terminal part of ANG II [5]. Losartan is well-absorbed orally and its hydroxymethyl group is rapidly converted via oxidation to carboxylate moiety in the human liver resulting to the potent metabolite EXP-3174, which extends the antihypertensive effects of the drug [6].

1.1. Conformational flexibility of losartan

In a previous study [7], we applied conformational analysis of losartan potassium in dimethyl sulfoxide (DMSO) using a combination of NMR spectroscopy and molecular modeling techniques. The flexible pharmacophore segments of losartan (Scheme 1) allow it to adopt many low energy conformers. In particular, the tetrazole and imidazole moieties may adopt an *anti* or *syn* orientation with respect to the A

* Corresponding author.
E-mail address: mzervou@eie.gr (M. Zervou).
[1] Current address: Bahcesehir University, Faculty of Medicine, Department of Biophysics, 34353 Istanbul, Turkey.

0005-2736/$ – see front matter © 2013 Elsevier B.V. All rights reserved.
http://dx.doi.org/10.1016/j.bbamem.2013.12.012

phenyl ring plane. Furthermore, the conformational flexibility of losartan is also mirrored in the positioning of the butyl chain either towards the tetrazole, possibly driven by C-H/π interactions, or away from it, pointing towards the opposite side of the space occupied by tetrazole with respect to the A phenyl ring plane (Fig. 1). Superimposition studies with the C-terminal segment of sarmesin, a competitive peptide antagonist of ANG II, showed an excellent fit with the *anti* configuration of the tetrazole and imidazole rings. [7]. The *anti* orientation was also determined in the crystals of losartan's anionic form grown in ethanol/water solution [8] or in aqueous solution [9], while the *syn* orientation was prevalent for the neutral form obtained in dioxan solution [10].

1.2. Interaction of losartan with membrane bilayers

Our previous studies employing Differential Scanning Calometry (DSC), ^{13}C Magic Angle Spinning (^{13}C MAS), and ^{31}P Cross-Polarization (^{31}P CP) solid state NMR spectroscopy in dipalmitoylphosphatidylcholine (DPPC) bilayers loaded with losartan have confirmed the interaction of losartan with this model lipid membrane. We observed that the drug interacts mainly with the interface region of the bilayer and anchors in the realm of the headgroup region. Moreover, molecular modeling studies of losartan in DPPC bilayers indicated the localization of the drug at the interface region favoring electrostatic interactions between the hydroxyl and tetrazole groups of the drug with the polar headgroups and diffusing water molecules [11–13]. The interaction of losartan with phospholipid membranes was further confirmed by Electron Spin Resonance (ESR) studies leading to the speculation that losartan may exert some of its effects through interaction with the lipids of the membrane bilayer besides its direct antagonistic action on the receptor [14]. This data is consistent with our proposed diffusion model according to which the favorable insertion of the drug into the interface is required for its diffusion towards the transmembrane (TM) active site of the AT_1 receptor [11].

1.3. Modeling of GPCRs and membrane diffusion hypothesis

The lack of crystallographic data for the human AT1 (hAT1) receptor and the notable flexibility of losartan has led to a discrepancy regarding the specific binding site and bioactive modes of the drug. The ligand binding site has been determined based on homology modeling of the hAT1 or the rat AT_1 receptors using structural models of rhodopsin

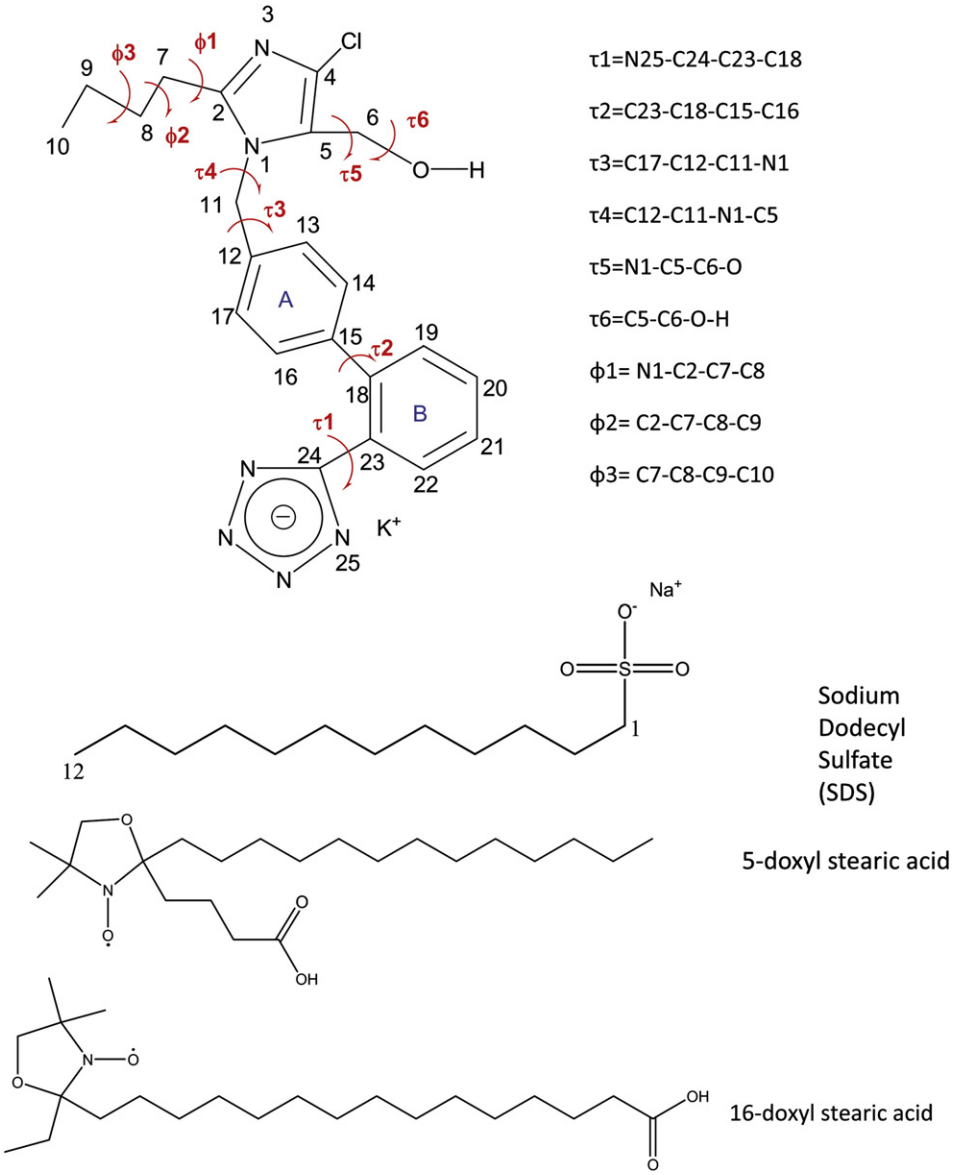

Scheme 1. Molecular structures of losartan, SDS, and of the spin-labeled 5- and 16-doxyl stearic acids. The critical dihedral angles of losartan that determine its conformational properties are also defined.

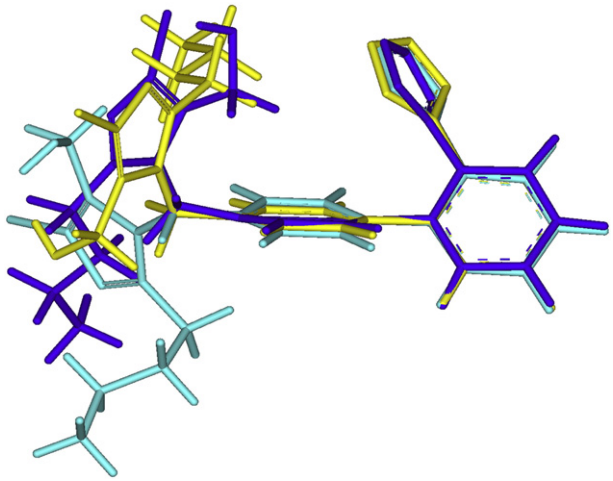

Fig. 1. Superimposition of one *anti* (crystal structure from [8] in cyan) and two *syn* (crystal structure from [9] in yellow and one theoretically derived low-energy conformer in blue) conformations of losartan, placing tetrazole and imidazole moieties in an *anti* or a *syn* orientation with respect to the A phenyl ring plane. The different butyl chain orientations either towards the tetrazole or away from it, pointing towards the opposite side of the A ring plane, are also depicted for the two *syn* conformers (yellow and blue respectively).

photointermediates and site-directed mutagenesis studies. The predicted binding site for sartans is located at the upper part of the receptor between the transmembrane helices 3–7 (TM3-7) and the extracellular loop 2 (ECL2) [15–17]. Moreover, mutational studies have revealed that ligand-specific conformational changes induced to the ECL2 are responsible for the switch between the active and inactive state of the receptor [18].

Recently, resolved crystal structures of the ligand activated turkey β1- and human β2-adrenergic, the human A2A-adenosine, the human dopamine D3 and the human chemokine CXCR4 GPCR class A receptors with antagonists bound, have identified structural differences with respect to the rhodopsin receptor. Open clefts in the extracellular regions may guide the entrance of the sartans towards the active site, whereas in rhodopsin the ECL-2 sits above the binding site and encloses it [19,20]. In line with this, the most recently developed homology model of AT1 based on the chemokine CXCR4 receptor, which was published after this study was performed, highlights the higher accessibility of the binding site to the extracellular environment [21,22].

Since sartans' pathway to approach the active site of AT_1 receptor has not been elucidated, both direct and membrane-mediated routes could underlie the drug action. Thus, the hypothesis of the lateral diffusion of the antagonist through the membrane in order to access the binding site merits further investigation.

1.4. Probing drug–membrane interactions

In this context, the molecular mechanism of drug:membrane interactions poses another issue of high significance for the design and screening of novel drugs. Partitioning of the ligand in the membrane driven by hydrophobic and electrostatic interactions is the primary mechanism of drug sequestration with a major impact in drug disposition [23]. Non-specific binding to the membrane or membrane-embedded receptors could hinder drug access to the binding site; however, diffusion through the membrane pathway could speed up the process of encountering the transmembrane binding site as compared to the random hit of the free ligand at the extracellular part of the receptor [24,25]. A complex interplay of all these factors will ultimately determine the overall drug efficacy. Lastly, membrane incorporation of drug molecules could possibly aid the ligand to adopt a bioactive conformation in order to interact effectively with a membrane embedded receptor target [24].

Phospholipids in the zwitterionic form comprise the most abundant class of lipid molecules found in cell membranes. The transbilayer distribution of the lipids across biological membranes is maintained to be asymmetric, which is a feature mediated by transporter proteins. Amine-containing phospholipids are found predominantly on the cytoplasmic surface of the plasma membrane while the concentration of choline-containing phospholipids and sphingolipids is higher on the extracellular membrane leaflet [28]. Furthermore, saturated phosphatildylcholine content is predominant ranging around 60% in vascular smooth muscle cell membranes, where the AT_1 receptor is localized among other tissues and organs [29]. Since the topography of the losartan binding site is localized in the outer monolayer as reported in the literature for modeled AT_1 receptors [15–17,22,30], DPPC was the lipid of choice for the AT_1/losartan/lipid bilayer Molecular Dynamics (MD) simulations implemented in this study.

In order to resolve drug:membrane interactions in atomic resolution, NMR spectroscopy techniques have been employed in various membrane-like environments including bicelles, vesicles, or micelles, which constitute the ideal membrane mimetic environment for providing well resolved NMR spectra, since the tumbling of the membrane-mimicking aggregates in solution is fast enough [26]. Detergent micelles as the anionic sodium dodecyl sulfate (SDS) and the zwitterionic dodecylphosphocholine (DPC) have been commonly used to resolve the 3D structure of membrane-interacting peptides and membrane proteins. However, certain drawbacks have been reported in the literature such as possible structural distortions induced by the spontaneous micelle curvature and the loss of functional folding due to detergent binding in the active site of the protein [27].

Our previous comparative biophysical studies of the sartan class drugs losartan and candesartan in membrane bilayers, have revealed a deeper insertion of losartan in DPPC bilayers, which has been attributed to its higher hydrophobic component, its weaker electrostatic interactions with the membrane surface (losartan features one negative charge due to its acidic tetrazole group as compared to the binary charge of candesartan due to both the acidic tetrazole and a carboxylate group), and its higher structural flexibility resulting in a more effective anchoring at the polar head groups and accommodation between the acyl chains [31].

The anionic detergent SDS, which encompasses structural characteristics that mimic the polar phosphate group and the long unbranched alkyl chains of the DPPC dipalmitoyl segment, was used in this study as a biomembrane-mimicking environment for the HR NMR studies. The use of anionic SDS micelles as a membrane mimetic aims to assess whether the hydrophobic contribution could compensate for the repulsive electrostatic interactions between the losartan tetrazole group and the micellar anionic head, enabling the association of losartan with micelles and spontaneous insertion in the hydrophobic core.

The interaction of valsartan, another member of the sartans, which bears two weakly acidic functionalities, with SDS micelles has been demonstrated previously; the study of losartan:SDS micelle interactions would enable us to directly compare the two antagonists interacting with membrane-mimicking systems [32,33].

In the current study, we performed a thorough conformational analysis of losartan by applying rotating frame nuclear Overhauser effect (2D ROESY) and nuclear Overhauser effect (2D NOESY) NMR spectroscopies in three different environments, mimicking conditions of biological transport fluids and membrane lipid bilayers. In particular, we have used water, the lower dielectric constant amphiphilic DMSO solvent mimicking the membrane headgroup/water interface, and ultimately SDS micellar solution, which additionally probes the hydrophobic interior of the bilayers. The calculated proton–proton distances were then applied as restraints to stochastic dynamics simulations using implicit solvation models in order to extract dynamic information about the pharmacophore arrangement of the molecule in the three studied environments. Drug association with micelles was followed with diffusion ordered spectroscopy (2D DOSY) spectroscopy and

drug:micelle intermolecular dipolar interactions were monitored by ROESY spectroscopy. Moreover, the topographical sites of the drug in the micellar environment were studied by introducing paramagnetic spin relaxation agents (i.e. 5-doxyl and 16-doxyl stearic acids) to the micelle solution and observing their effect on the drug resonances. The unprompted insertion, the diffusion pathway and dynamics of losartan were monitored by Molecular Dynamics (MD) simulations in a modeled micellar aggregate environment [34] and a long exploratory MD run (580 ns) in a DPPC bilayer [35] with the AT_1 receptor embedded [16,36]. This integrated approach aims to investigate the impact of membranes in losartan's pathway towards the AT_1 receptor.

2. Experimental section

Losartan potassium was kindly donated by Merck. Deuterated and protonated sodium dodecyl sulfate SDS-d_{25} and SDS-H_{25} respectively, and the spin labels 5- and 16-doxylstearate were purchased from SIGMA.

2.1. NMR samples preparation

Losartan was studied in DMSO-d_6, D_2O, and micellar solutions in two different concentrations, 5 and 15 mM. The pD values in the aqueous solutions were 7.8 (5 mM) and 8.2 (15 mM).

The partitioning of the drug in the micellar systems was studied by adding 5 mM losartan in 400 mM SDS-d_{25}/D_2O solution (drug:micelle preparation A). The preparation was subjected to sonication to provide a transparent solution. SDS concentration exceeded the critical micelle concentration (CMC = 8.2 mM) in order to ensure micelle formation and the applied molar ratio (drug:micelle = 1:80) was used to establish the immersion of at least one drug molecule in the micellar aggregate assuming an SDS aggregation number of at least 60 monomers [37]. The pD value in the micellar environment was 8.8. To determine the location of losartan in the micelle, 5-DSA and 16-DSA water solutions of 50 μL were prepared in a molar ratio of 1:4 (spin label:drug) according to Ref. [38]. Successive aliquots of 5 μL of each DSA were added in separate drug:micelle solutions.

In order to elucidate drug:micelle intermolecular interactions, D_2O solutions of 15 mM losartan in 200 mM SDS-H_{25} or 200 mM SDS-d_{25} were also prepared (drug:micelle preparations B). The pD values of the solutions were 9.3 (15 mM drug:200 mM SDS-H_{25}) and 9.8 (15 mM drug:200 mM SDS-d_{25}).

At the given experimental conditions, SDS (pKa = 1.9) and the acidic tetrazole of losartan (pKa = 5.5) were deprotonated.

2.2. NMR spectroscopy

NMR spectra of losartan in the three various environments were recorded on Varian 600 MHz spectrometers. 2D NMR experiments as DQF-COSY, ^1H–^{13}C HSQC and ^1H–^{13}C HMBC confirmed the resonances assignment. A series of NOESY experiments in DMSO using mixing times of 75 ms, 150 ms, 300 ms and 1 s revealed that the mixing time of 150 ms could ensure the operation at the initial linear part of the NOE buildup curve. 2D NOESY and ROESY experiments were performed using a mixing time of 150 ms in the phase-sensitive mode and the WET sequence to suppress the water signal in the aqueous and micellar solutions. ROESY spectra were acquired using 4 KHz spin-locking field strength. Interatomic proton–proton distances were calculated using the two-spin approximation and the integrated cross peaks intensity of a pair of adjacent aromatic protons assumed to have a distance of 2.46 Å. The resulting distances were corrected for the frequency offset [39]. Upper and lower limit constraints were estimated as ± 10% of the resulted value.

DOSY experiments were recorded at 298 K using the Bipolar Pulse Pair Stimulated Echo (Dbppste) pulse sequence of Varian library with a gradient duration of 2 ms, a diffusion delay of 50 ms and an array of 15 values for gradient strength varying between 1000 and 25,000 G cm^{-1}. Spectra were processed using the Bayesian DOSY transform implemented in Mnova s/w. The uncertainty of the translational diffusion constant D has been evaluated to 10% based on the average error estimation of the diffusion coefficients of the distinct resonance peaks as performed in VnmrJ analysis routines.

2.3. Molecular modeling

2.3.1. Molecular modeling in implicit solvent

MD simulations were performed using the Stochastic Dynamics method of the Maestro (v.9.5) MacroModel module [40] and the OPLS-2005 force field. The simulation temperature was 300 K in order to mimic the spectroscopic experimental conditions. Solvent effects were simulated using the Generalized Born/Surface Area (GB/SA) solvation model and setting the values of the dielectric constant ε = 45, 80 and 32 for DMSO, water, and SDS micellar environments, respectively. The choice of the dielectric constant for the micellar environment was based on literature data determined from pyrene fluorescence spectroscopic measurements in SDS micelles in the absence of NaCl [41]. The applied dielectric constant is also in a good agreement with an estimate of the polarity of the interface between lipid bilayers and bulk aqueous solution (ε ~ 35) [42].

The crystallographically-determined structures of losartan [8–10] were used as initial ligand conformations. The MD runs included a stage of 2 ns equilibration and 10 ns simulation. The integration time-step was set to 1 fs. Unconstrained and constrained MD simulations were performed and in the case of the latter, NMR derived distance restraints were applied with a force constant of 3 kcal mol^{-1} $Å^{-1}$ and a (± 10%) uncertainty. All critical dihedral angles were monitored during the simulation.

A grid scan search was used to explore the energy landscape of the drug by systematically varying the critical dihedrals τ_2 and τ_3 by 10° using the Coordinate Scan algorithm of the MacroModel module [40].

2.3.2. Molecular modeling in SDS micelles

The initial coordinates of a pre-equilibrated micelle structure of 60 SDS molecules were kindly provided by Prof. Alexander MacKerell [34]. The initial model system was fully minimized with Molecular Mechanics (MM) using MacroModel 9.5 [40] and the OPLS-2005 force field, implicit water solvent (GB/SA continuum solvation treatment), and extended non-bonded cutoff. The minimization was carried out using the Polak–Ribiere Conjugate Gradient (PRCG) method with convergence movement threshold of 0.001 kJ mol^{-1} $Å^{-1}$.

Following the relaxation of the micelle structure, the losartan anionic form was placed randomly ~5 Å away from the micelle surface. The merged system was solvated in an orthorhombic simulation buffer box of size 20 Å in each direction with 17363 TIP4P water molecules and 61 sodium counterions, randomly distributed in the aqueous phase.

MD simulations were performed with Desmond 3.1 [43] using the OPLS 2005 force field. Before the production run, the model system was relaxed through a series of minimizations and short MD simulations were performed using Desmond default values. Production runs were performed in the NPT ensemble at 300 K and 1.01325 bar with periodic boundary conditions for 20 ns. The RESPA integrator [44] was used with time step 2 fs for bonded and short-range interactions and 6 fs for long-range interactions. During equilibration the Berendsen thermostat and barostat [45] were applied with coupling time constants of 100 ps and 1000 ps, respectively. The cutoff distance for the Coulombic interactions was set to 9 Å, while the long range Coulombic interactions were calculated using the smooth Particle Mesh Ewald (PME) method [46] with a tolerance of 1e-09. Visualization of the trajectories was performed using Maestro (Schrödinger, LLC) [47]. The calculation of the distance between the center of masses of losartan and the micelle throughout the trajectories was performed with the "center of mass" (COM) and "distance states" scripts of PyMOL [48].

2.3.3. Molecular modeling of phospholipid bilayers with the AT_1 embedded receptor

The topology and the coordinates of a pre-equilibrated 128 DPPC lipid bilayer were downloaded from Peter Tieleman's Biocomputing Group website [35]. The 128-DPPC lipid bilayer was replicated along the xy plane to produce a membrane of 512 DPPC lipids. The resulting system was subjected to 500 steps of Steepest Descent (SD) energy minimization followed by an equilibration of 10 ns MD simulation with the GROMACS 4.5.4 package and the GROMOS 53a6 force field [49,50]. The area per lipid of the bilayer reached a plateau after 4 ns at 61 ± 0.4 $Å^2$, which agrees very well with the experimental value of 63 $Å^2$ [51]. The bilayer structure from the last snapshot of this simulation was extracted, placed in a 12.5 × 12.5 × 11 nm rectangular box, and solvated. The new system was subjected to a 200 ps MD run before inserting the modeled AT_1 receptor [16]. The protein was then embedded into the membrane employing the protocol implemented in the GROMACS script g_membed [52]. Briefly, the size of the protein is scaled by a factor of 0.5 in the membrane plane. All lipid and solvent molecules overlapping with the resized protein were removed and an MD step is performed with all intra-protein interactions turned off. Then, the resize factor is incremented by a small amount and the protein is resized again followed by another MD step. This procedure is iterated 1000 times until the protein reaches its original size. In total, 28 DPPC lipid molecules were removed yielding a lipid bilayer of 484 DPPC lipid molecules evenly distributed in the two leaflets. Subsequently, eight losartan molecules were added to the system. Special care was taken so as to place losartan molecules in different positions in the simulation box: four of them were placed in the water phase, two at the lipid–water interface and two in the interior of the DPPC bilayer. All losartan molecules were placed randomly at a distance at least 20 Å away from the receptor. The system was then neutralized by adding a sufficient number of Cl^- counter ions. The size of the final AT1/DPPC/Water/8losartan/Cl^- system was 136,781 atoms. After an energy minimization using the Steepest Descent method, the system was subjected to a 2 ns MD simulation applying harmonic positional restraints (1000 kJ/mol/nm^2) on all protein atoms to allow equilibration of the protein–lipid interface, followed by a 5 ns MD simulation run with the protein restraints removed. Finally, a 580 ns production run was carried out. To ensure proper convergence of the system properties, the first 100 ns of the simulation were discarded as equilibration.

All energy minimizations and MD simulations were performed with GROMACS 4.5.4 software package using the GROMOS 53a6 force field updated with the Berger lipid parameters. The SPC water model was used and standard GROMOS parameters for losartan were obtained from the PRODRG server [53]. The bond parameters for the C – Cl bond resulting from the PRODRG server were different from the standard GROMOS parameters. Therefore, these were altered to the original GROMOS C – Cl parameters (bond length: 0.176 nm, bond force constant: 8,100,000 kJ/mol/nm^2). All other parameters were left unchanged. Harmonic restraints (600 kJ/mol/rad^2) on the improper dihedrals of losartan were placed to ensure ring planarity. Moreover, due to the fact that partial atomic charges generated by PRODRG are not compatible with GROMOS force fields [54], the losartan atomic charges were determined from fitting the quantum mechanical electrostatic potential of the molecule using the package NWChem 6.0 [55,56]. In these calculations, the total charge imposed on losartan was zero and the sum of the atomic charges in the tetrazole, imidazole, methyl, and two phenyl groups was constrained to zero following the GROMOS force field conventions for the definition of charge groups. All bonded and non-bonded parameters of losartan were tested by running a 5 ns MD simulation of the molecule in vacuo in which the conformational flexibility of its chemical groups was visually examined. MD simulations of the AT1/DPPC/Water/Losartan system were run in the NPT ensemble at 323 K and 1 bar with periodic boundary conditions. The leap-frog integrator was used to solve the equations of motion with a 2 fs integration time step. The temperature of the system was controlled with the Nose–Hoover thermostat and a coupling time constant of 0.5 ps. The Parrinello–Raman barostat with a coupling time constant of 5 ps was used to control pressure. Electrostatic interactions were calculated with the PME method using a 1.4 nm cutoff for the direct space sum. For the van der Waals interactions, the Lennard–Jones potential was smoothly switched off from 0.8 to 1.2 nm. All bonds were constrained using the LINCS algorithm.

3. Results and discussion

3.1. NMR spectroscopy

Structural elucidation and conformational analysis of losartan in DMSO have been already reported in a previous publication [7]. The current study investigates further the conformational features of the drug in the aqueous and SDS micellar environments. Two different concentrations of the drug, namely 5 and 15 mM were examined relatively to their NMR profiling in the different environments. Chemical shift variations as well as differentiation of the B aromatic ring pattern were observed between the different concentrations of the drug in aqueous solution, while the DMSO and micellar environment profilings showed no concentration dependence.

^{1}H NMR spectra of the drug in DMSO, D_2O and SDS micelles are shown in Fig. 2 and Table 1 displays ^{1}H NMR chemical shifts of losartan at the two concentrations used 5 mM and 15 mM in the three different environments.

3.1.1. Comparison of the ^{1}H NMR profiling of losartan in the different environments

Inspection of the 5 mM ^{1}H NMR spectral patterns of the drug in the three different environments (i) DMSO, (ii) D_2O, and (iv) SDS displayed in Fig. 2 reveals that the higher polarity of D_2O causes an upfield shift, relative to the amphiphilic DMSO and micellar solutions, of the alkyl chain and A phenyl ring protons, ranging between 0.1 and 0.15 ppm. However, this tendency is not observed for phenyl ring B with the exception of H22 adjacent to the tetrazole anion.

The upfield shift of the alkyl chain and the A ring protons in the aqueous environment is probably associated with a conformational redistribution, which may lead to an increase of *gauche* conformations of the alkyl chain as well as to the involvement of CH–π interactions [57,58]. Furthermore, the dipolar interactions between water molecules and the tetrazole ring could induce the observed shielding of the neighboring H22.

The hydrogen bond acceptor DMSO appears to induce hydrogen bonding with the imidazole hydroxyl group, which is supported by the presence of the –OH resonance peak shifted towards higher frequency scale (at 5.2 ppm) and by the observed splitting pattern of this peak (triplet, J = 5.3 Hz) in combination with the doublet coupling pattern of methylene H6. This coupling, present only in the DMSO environment, may result from the increased stability and slow exchange rate of the hydroxyl proton.

Evidence for a concentration dependent self-assembly behavior of losartan in aqueous environment is provided by (a) ^{1}H NMR profile differentiation, (b) Transverse relaxation (T_2) time measurements, and (c) DOSY spectroscopy.

^{1}H NMR profile differentiation. Increase of the concentration in aqueous solution from 5 mM to 15 mM (Fig. 2 ii and iii, respectively) increases further the upfield shift of the resonances and alters the B ring ^{1}H profile. The difference in pD between the two studied concentrations of losartan cannot account for the observed significant chemical shift changes. Such a concentration dependence of the chemical shifts in D_2O has been reported in the literature for systems bearing unprotonated nitrogen heterocycles, and has been attributed to aromatic stacking behavior and subsequent aggregation [59].

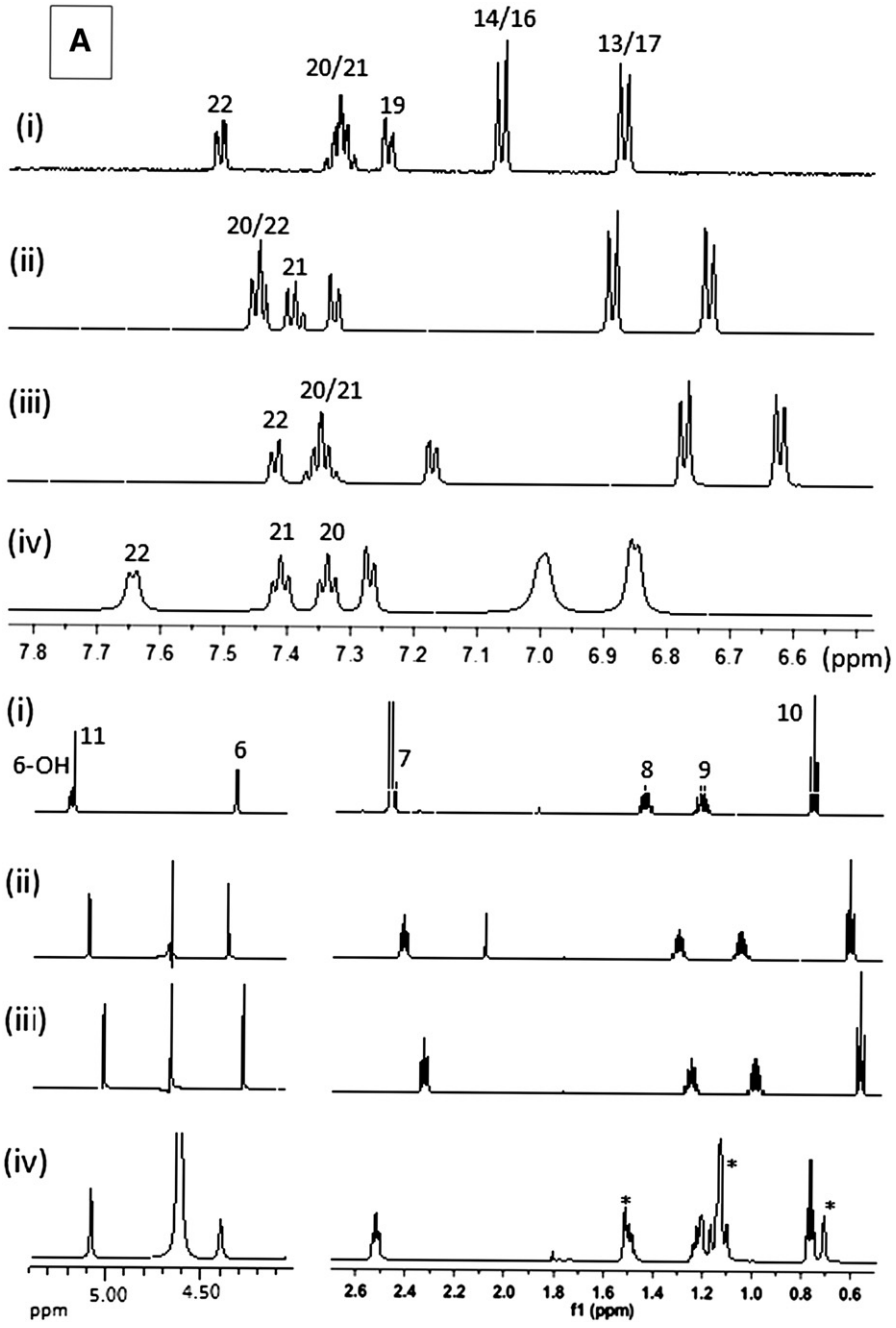

Fig. 2. ^{1}H NMR representative spectra of losartan (upper part: aromatic and lower part: aliphatic region). (i) 5 mM in DMSO-d_6 (ii) 5 mM in D_2O (iii) 15 mM in D_2O (iv) 5 mM in SDS-d_{25} micelles solution. Additional peaks in the alkyl region of losartan in micelles (denoted with *) are due to residual protons of SDS-d_{25}.

Transverse relaxation (T_2) *time measurements* revealed a notable decrease of the B aromatic ring mobility associated with the increased concentration in D_2O solution. This decrease in mobility is particularly prominent for proton H19 (93% decrease) (Supplementary Material, Fig. S1) and presents an additional indication for the formation of assemblies as the concentration increases. The presence of K^+ ions in the solution could possibly induce the formation of assemblies with the ionized losartan tetrazole moieties. Such interactions impose limitations to the mobility of the tetrazole ring and further to the adjacent phenyl ring. Coordination patterns have been reported for the crystal structures of losartan potassium [8,9].

DOSY spectroscopy has been established as a new method to detect the presence of assemblies. Interpretation of DOSY data for the two drug concentrations in aqueous solution (Fig. 3a and b) revealed a higher diffusion constant associated with the 5 mM concentration ($D = 2.6 \pm 0.3 \times 10^{-10}$ m^2 s^{-1}). The more concentrated solution (15 mM) displayed a double series of traces with lower constants ($D = 2.3 \pm 0.2 \times 10^{-10}$ m^2 s^{-1} and $D = 2.0 \pm 0.2 \times 10^{-10}$ m^2 s^{-1}) in a ratio of 4.6:1, implying the formation of assemblies comprised of different number of losartan molecules, resonating in an average chemical shift. The obtained experimental data corroborate with the assumption of concentration dependent self-assembly behavior of losartan in aqueous environment possibly associated with the anionic tetrazole and the presence of K^+ counterions in the solution. Interestingly, no concentration dependence of the chemical shifts, neither of the transverse relaxation times, nor of the self-diffusion coefficient was observed for the aqueous solution of the AT_1 antagonist valsartan, which bears a protonated tetrazole ring [32]. Furthermore, the potent metabolite of losartan, EXP-3174, which was studied in its neutral form in DMSO and in aqueous solutions, exhibited a similarly well resolved B

Table 1
^{1}H NMR chemical shifts of losartan in DMSO-d_6, D_2O and micelles. Two different concentrations were studied, 5 mM and 15 mM. Chemical shift variations were only observed in aqueous environment.

Atoms	Losartan in different environments			
	DMSO 5 mM/15 mM	D_2O		Micelles 5 mM/15 mM
		5 mM	15 mM	
H10	0.78 t	0.62 t	0.58	0.77
H9	1.23-sextet	1.6-sextet	1.0	1.22
H8	1.45-quintet	1.31	1.26	1.5
H7	2.47 t	2.4	2.32	2.52
H6	4.29d	4.32 s	4.24	4.39
H11	5.80 s	5.08 s	5.0	5.15
OH	5.2 t	–	–	–
H-13/17	6.87d	6.73d	6.63d	6.85d
H-14/16	7.06d	6.89d	6.79	6.99
H19	7.24dd	7.32d	7.17dd	7.27d
H20	7.32 m	7.45 m	7.6 m	7.34 t
H21	7.32 m	7.9 t	7.36 m	7.41 t
H22	7.51dd	7.45 m	7.44dd	7.64d
Reference	DMSO: 2.49		D_2O: 4.7	

ring ^{1}H profile at both concentrations of 5 mM and 15 mM. The corresponding spectra obtained at the increased concentration are presented in Fig. S2 of the Supplementary material.

3.1.2. Association of losartan with micelles

In order to exclude any self-assembly effects, a drug concentration of 5 mM was chosen for the study of losartan interaction with micelles. An excess concentration of 400 mM was used for the micelle aiming to ensure the immersion of at least one drug molecule in the detergent aggregates. The increase of the ^{1}H NMR linewidth compared to the water solution, indicated the interaction of the drug with micelles (Fig. 2, iv). Diffusion experiments also confirmed the association of the drug molecules with the micellar aggregate. More specifically, the insertion of the drug in the micellar environment was accompanied by a reduction of the diffusion coefficient ($D = 4.3 \pm 0.4 \times 10^{-11}$ m^2 s^{-1}) (Fig. 3d), which is one order of magnitude less than the aqueous or DMSO environment ($D = 1.6 \pm 0.2 \times 10^{-10}$ m^2 s^{-1}) (Fig. 3c). Inspection of a single set of ^{1}H resonance lines as well as the observation of a single series of DOSY traces corroborate with a fast chemical exchange between the free and the micelle-bound states of the drug. Thus, the calculated diffusion coefficient reflects the average value of the two exchanging entities.

The mobility of losartan in the micellar environment was also investigated through transverse relaxation measurements. The notable decrease of spin–spin relaxation time compared to the aqueous solution is indicative of the affinity of losartan to SDS micelles. In addition, the similarity in T_2 values as measured for all resonance peaks indicates that all moieties of the molecule interact with the micelle (Supplementary Material, Fig. S1). In the amphiphilic DMSO environment, the transverse relaxation times are comparable to those in the micellar environment with the exception of the terminal methyl H10 and the spacer methylene H11, which retain their flexibility (Supplementary Material, Fig. S1).

3.1.2.1. Use of spin labels to locate losartan in the micellar environment. To determine the drug topography in the micellar aggregate, solution NMR relaxation probes were used. The 5-doxylstearate (5-DSA) spin label bears a nitroxide near the head of the stearate and induces relaxation of the NMR signals of the drug moieties in the proximity of the micelle surface, while 16-doxylstearate (16-DSA) spin label has a nitroxide near the end of the alkyl chain of the stearate and affects the resonances of losartan protons located deep in the hydrophobic region of the

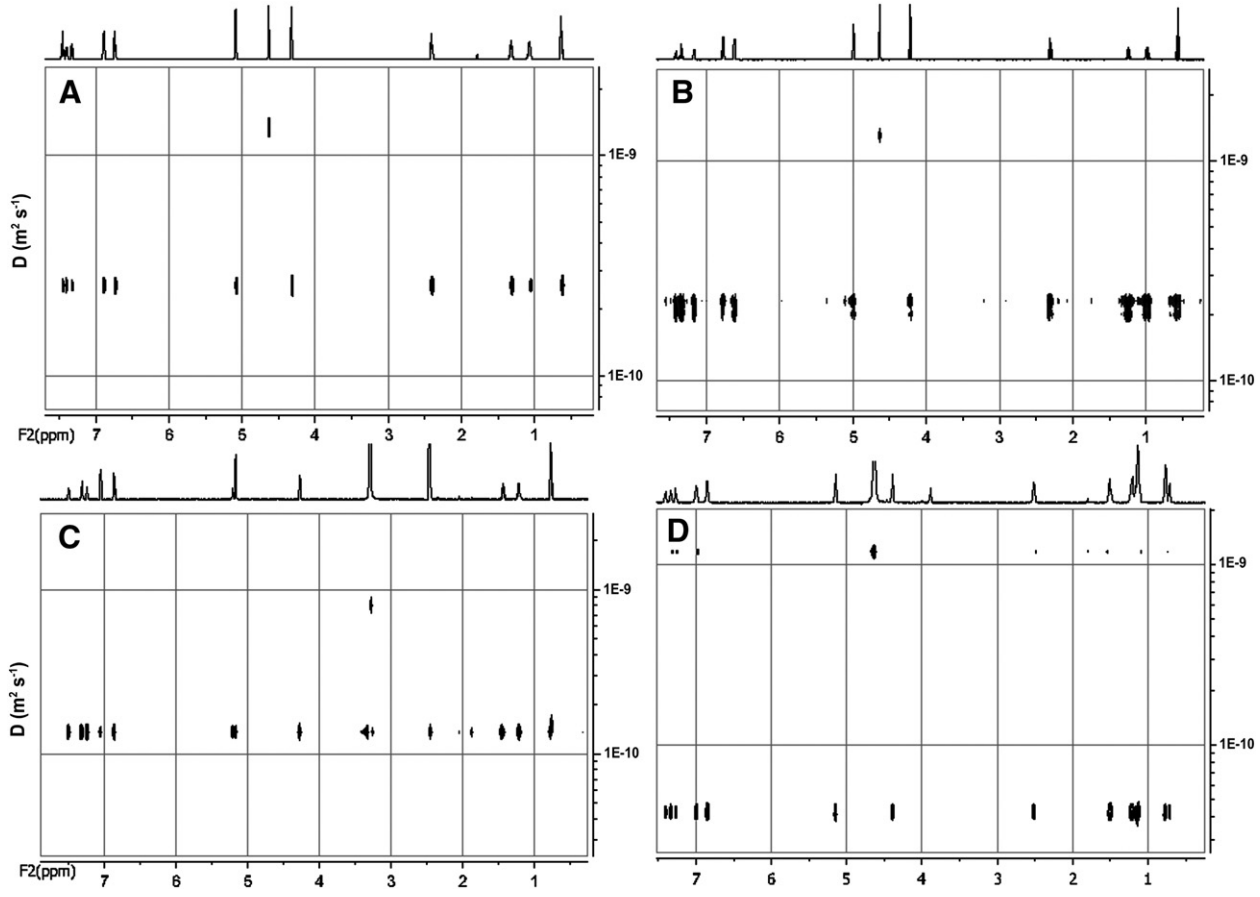

Fig. 3. DOSY spectra of (a) 5 mM Los in D_2O (b) 15 mM Los in D_2O (c) 5 mM Los in DMSO-d_6 (d) 5 mM Los in 400 mM SDS-d_{25}.

micelles [59]. Successive additions of 5-DSA or 16-DSA were added to micellar solutions in an effort to keep a satisfactory S/N for a reasonable observation of the distinct resonances.

Resonance peaks were deconvoluted and the calculated half widths were used to report the paramagnetic broadening upon the successive additions of 5-DSA and 16-DSA. The chart in Fig. 4 displays the variation of the half linewidth for characteristic resonance peaks representing the different functionalities of the drug as the alkyl chain (methylenes H7 and methyl H10), the methanol protons H6, the spacer methylene H11, the A aromatic ring (H13/17), and the B aromatic ring (H19, H20 and H22).

The incorporation of 5-DSA free radical showed a notable increase of half-width of the alkyl chain peaks as well as of the B ring protons H19, H20 and a less pronounced broadening of the A ring protons, of the methylenes H11 and H6, and the B ring proton H22.

The paramagnetic effect of 16-DSA located deep in the hydrophobic segment of micelles is clearly reduced compared with 5-DSA. In this case, alkyl chain protons and specifically the final methyl and the B ring protons H19 and H20 are more susceptible to the presence of the nitroxide spin label. To a lesser degree the resonances of the A ring H13/17 and methylene H11 are also influenced. Notably, the effect upon the resonance lines of H6 and H22 is practically negligible.

The obtained results support a location of losartan near the micellar surface since the interaction with 5-DSA is notably more prominent than the one with 16-DSA. Furthermore, evidence of the preferred orientation of losartan's pharmacophores is also provided. Specifically, the hydroxymethyl group and B ring proton H22 adjacent to the tetrazole face the micelle–water interface, whereas the butyl chain and the B ring protons H19 and H20 are interacting with the hydrophobic center of the micelle. These experimental data do not indicate preference for the *anti* or *syn* conformation in the detergent environment; however an arrangement of the butyl chain towards the micellar core is confirmed.

3.1.2.2. Probing drug:micelles intermolecular interactions. In an effort to elucidate further the drug:micellar aggregates interaction sites, ROESY cross relaxation experiments have been carried out. A drug concentration of 15 mM in D_2O solutions of 200 mM SDS-H_{25} or 200 mM SDS-d_{25} (drug:micelle preparations B) was used. Fig. 5 displays overlaid corresponding regions from the experiments with the protonated and the perdeuterated detergent, enabling the discrimination between the intra- and inter-molecular interactions of losartan. SDS resonance lines have been assigned according to the reference [59].

Strong intermolecular ROEs are observed between the two aromatic rings, the spacer methylene H11, the hydroxymethyl H6 as well as the alkyl chain methylene H7 and SDS protons S_{3-11}, which are attached to the third carbon after the sulfate group till the penultimate one. The evaluation of the ROEs intensities can only be qualitative due to the extensive spin diffusion along the detergent alkyl chain. Moreover, severe overlap with the SDS resonance lines obscured possible ROE signals with the rest of the butyl chain of losartan. The obtained results though indicate clearly that losartan is distributed in the vicinity of the hydrocarbon chains.

Furthermore, the protons of the A ring (H13/17 and H14/16) as well as the methylene H7 appear to be in contact with SDS proton S_2 attached to the second carbon after the sulfate group, providing evidence that losartan is also interacting with the head groups of the micelle. Although the terminal SDS methyl S_{12} overlaps with losartan butyl chain methyl H10 preventing definite conclusions, a lack of observed NOEs between the B aromatic ring and hydroxymethyl protons H6 with S_{12} further supports their orientation towards the polar headgroup of the micelles.

Valsartan was also observed to interact strongly with the aliphatic chain of SDS S_{3-11}. However, the lack of intermolecular NOEs with the S_2 position of the detergent most probably indicates a deeper insertion of valsartan relatively to losartan [32].

3.1.3. NOE connectivities and conformational analysis of the drug in the different environments

In an effort to elucidate the conformational differences of the molecule in the three different studied environments, quantification of the interatomic distances was deemed necessary. Thus, NMR spectroscopic studies using the ROESY/NOESY methods have been repeated for losartan in DMSO and extended to aqueous and micellar environments. A drug concentration of 5 mM was used in all cases and the micelle was formed by 400 mM SDS-d_{25} in D_2O solution (drug:micelle preparation A). Integration of ROE and NOE cross peak signals gave similar results. The corresponding ROESY spectra are provided at the Supplementary Material (Supplementary Material, Fig. S3–S5) and the calculated interatomic distances are shown in Table 2.

The striking difference between the three studied environments is reflected in the flexibility of the butyl chain. The plethora of ROEs observed in DMSO or micelles between the chain protons and the A ring (i.e. H7, H8, H9 with H13/17) as well as between the chain protons and the spacer methylene (H8, H9 with protons H11) suggest a predominant arrangement of the chain in a close proximity with the A ring.

The greater flexibility of the alkyl chain in the aqueous environment is reflected by the absence of characteristic ROEs (i.e. between H9 and H11 or between H9 and A ring protons). The enhanced conformational mobility of the chain in the aqueous environment has also been observed by crystallographic studies of losartan potassium. It was suggested that while biphenyltetrazole moieties form coordination interactions mediated by K^+ cations, the atoms of the chain and the imidazole ring except the oxygen atom, which also participates in the coordination sphere of the metal ion, are highly agitated and disordered [9].

In agreement with the relaxation time measurements, the conformational flexibility of the drug in DMSO and micellar environments

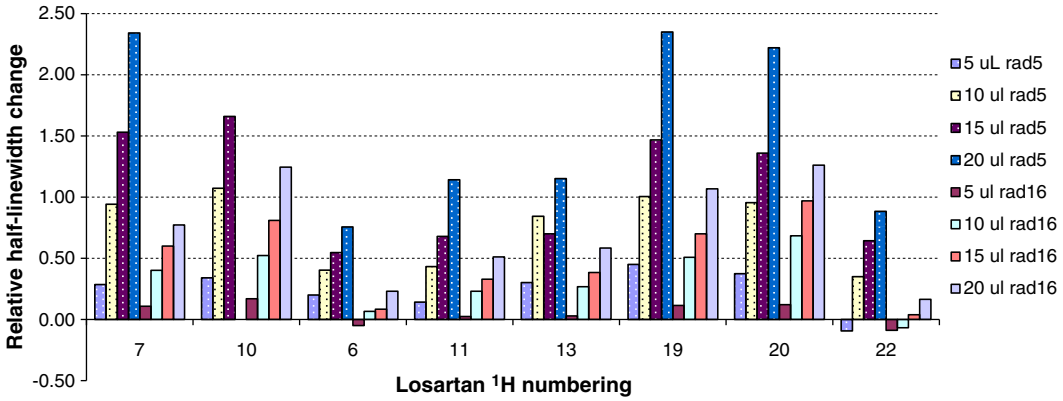

Fig. 4. Broadening of half linewidth of losartan resonance peaks (relative half linewidth change) upon successive additions of 5-DSA denoted as rad5 (dot bar graphs) and 16DSA denoted as rad16 in the micellar solution in a molar ratio of 1:4 (spin label:drug). * The absence of the broadening bar for methyl protons H10 at the 4th addition of 16-DSA is due to serious distortion of the lineshape.

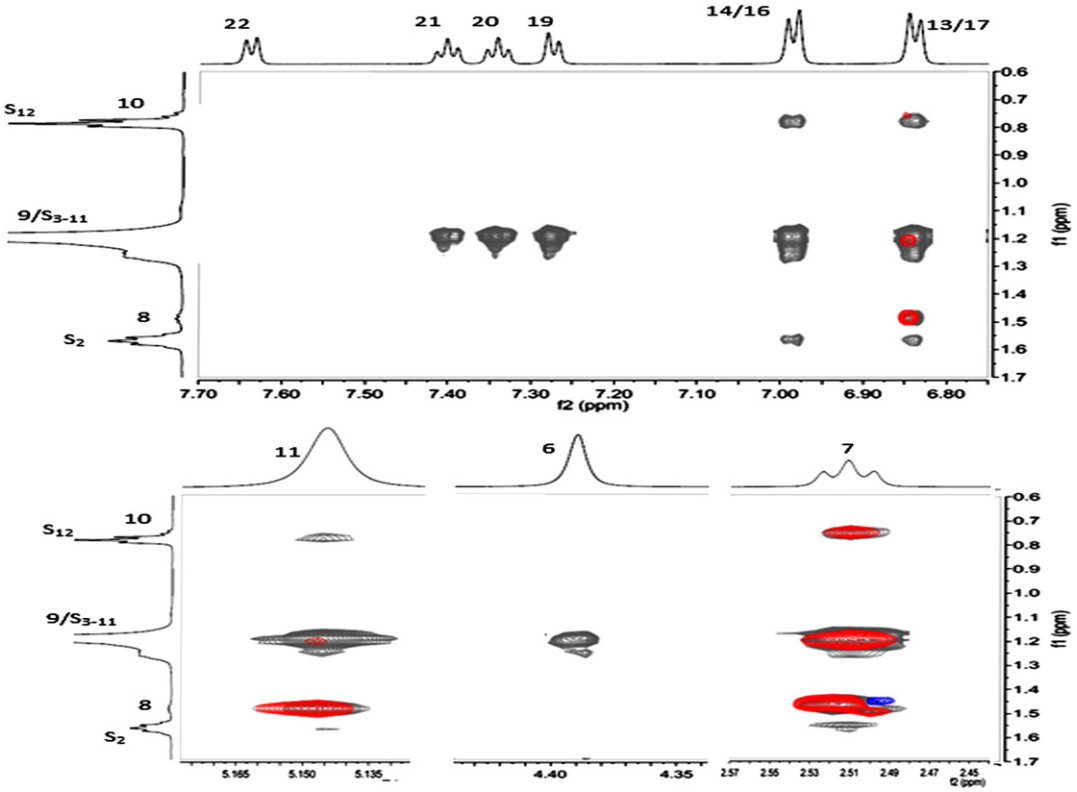

Fig. 5. ROE interactions between the drug and the micelle. Overlaid are expanded regions from the spectra of 15 mM losartan in 200 mM SDS-H_{25} (gray traces) and in SDS-d_{25} (red traces). The mixing time used was 150 ms. The depicted horizontal and vertical 1D traces correspond to the protonated detergent solution.

emerges to be very similar. Moreover, the decreased mobility of the alkyl chain in the micelles with respect to bulk water indicates that the drug:membrane interactions and the diffusion mechanism through the biological membrane, mimicked in the current study by micelle aggregates, contributes to the reduction of the entropy of losartan while it diffuses through the membrane to the receptor site.

3.2. MD simulations

3.2.1. MD simulations of losartan in implicit solvation environments

The experimentally derived interatomic distances could not determine unambiguously whether the *anti* or *syn* configuration of the drug is the predominant one in solution. Thus, in a further step, we investigated the dynamic stability of the various energetically favorable conformers by applying MD simulations using implicit solvation method for the three studied environments (DMSO, D_2O, SDS micelles).

Different initial conformations of the drug, including all crystallographically determined structures [8–10], were subjected to unconstrained and constrained MD simulations using the NMR derived interatomic distances as restraints.

Analysis of the trajectories in all studied implicit solvation environments supports the following conclusions: (a) Unconstrained MD simulations reveal the prevalence of the *syn* configuration throughout the simulation time; (b) Restraining the flexibility of

Table 2
Interatomic proton–proton distances (Å) derived from ROESY spectra for losartan in different solvents and in micelles. Comparison with the average values of the distances measured throughout the course of MD simulations in micelles and in DPPC lipid bilayer with the AT_1 receptor embedded. The values calculated from the DPPC:losartan:AT_1 system were cut off at 5 Å in order to correspond to the experimentally-measured values.

Losartan atoms		Experimental interatomic distances (calculated from ROE data with a st. dev. of ±10%)			Average values calculated during the course of MD simulations		
		5 mM losartan in			Micelles		Lipid bilayers
		DMSO	D_2O	400 mM SDS-*d25*	*Anti* initial conformer	*Syn* initial conformer	Average of the 8 losartan molecules
10	7	3.4	3.7	3.4	3.9	3.9	3.6 (0.3)
10	8	3.1	3.4	2.6	2.6	2.6	2.5 (0.1)
9	7	2.8	3	2.6	2.6	2.6	2.5 (0.1)
9	11	3.6	–	3.7	4.5	5.0	5.1 (0.4)
9	13/17	3.7	–	3.6	4.8	4.5	4.5 (0.3)
8	11	3	3	3	3.9	4	4.1 (0.3)
8	13/17	3.4	3.5	3.5	4.2	4.5	4.4 (0.4)
7	11	2.2	2.3	2.2	2.3	2.3	3.1 (0.1)
7	13/17	3.1	3	3	3.5	3.5	4.0 (0.4)/4.1 (0.4)
6	11	2.5	2.3	2.6	3.5	3	3.1 (0.1)
6	13/17	2.8	2.9	3	3.4	3.6	4.1 (0.4)/4.0 (0.6)
11	13/17	2.4	2.6	2.6	2.8	2.4	2.4 (0.04)
19	14/16	2.5	2.6	2.7	3.5	3.5	3.2 (0.1)

the imidazole moiety by imposing NOE constraints between H6–H11 and between H6–H13/17 is the prerequisite for the dynamic stability of the *anti* conformation issuing a smooth potential energy curve along the MD simulation although the energy is ~7 kcal mol^{-1} higher with respect to the unconstrained MD; (c) The conversion of the *anti* to *syn* conformation was not hindered by imposing a distance constraint between H14/16–H19, thus restraining τ_2 dihedral.

The last two observations indicated that the interconversion should rely solely on the rotation around the critical torsion angle τ_3. To investigate further the energetic cost of this transition, a grid scan search was performed by systematically varying the dihedrals τ_2 and τ_3. As observed from the heat map of Fig. 6 the energy minima are located symmetrically at $\tau_2 = 60°$ and 120° indicating the unobstructed fluctuation of the phenyl-tetrazole moiety around the vertical position with respect to the neighboring A phenyl ring. As a general rule, the *anti* conformers bear the torsions τ_2 and τ_3 with the same sign, while the *syn* conformers adopt opposite sign for those angles. As already shown in our previous publication [7], the transition from the *anti* to *syn* by rotation around τ_2 (i.e. moving from conformer A towards conformer C following a trajectory parallel to dihedral τ_2 axis) is extremely energy demanding since a barrier of 8 kcal mol^{-1} needs to be overcome. On the other hand, the energy profiles of Fig. 6 reveal that the interconversion between the *syn* and *anti* conformations is notably more energetically favorable by rotation around τ_3 since the energy barrier to be overcome is ~2 kcal mol^{-1} (i.e. transition from conformer B to conformer C moving parallel to the dihedral τ_3 axis). Moreover, unhindered rotation around τ_3 influences the positioning of the butyl chain drifting it above the A ring plane (i.e. conformations B and C in Fig. 6) or below the plane (i.e. conformations A and D in Fig. 6) in the same or opposite side of the space occupied by tetrazole, respectively.

3.2.2. MD simulations of losartan-loaded SDS

MD simulations were run with the losartan anionic form (both *syn* and *anti* orientations of the tetrazole with respect to the imidazole) placed randomly ~5 Å away from the surface of SDS aggregates in the aqueous environment. The drug was placed in the aqueous environment in order to study i) its spontaneous insertion into the micelle and further diffusion into the micelle core and ii) potential conformational changes induced by its interaction with the micelle.

MD simulations show that both conformers (*syn* and *anti*) approach the micelle surface very quickly (in the first 2 ns of the simulation time) and diffuse between the polar headgroups and the upper part of the alkyl chains of SDS (Fig. 7). This localization favors the formation of hydrogen bond interactions between the hydroxyl group of losartan and the sulfate group of SDS as was observed in approx. 20% of the trajectories frames collected from the MD simulations.

In Fig. 8, the approach of the drug into the micellar interface is graphically represented by the plot of the distance between the center of masses of losartan and of micelle versus the simulation time.

Interestingly, the conformational behavior of *syn* and *anti* orientations of the drug throughout the MD simulations is different. The *anti* conformer is preserved during most of the simulation time as depicted in Fig. 9A. On the other hand, the *syn* conformer is exchanging between the 2 states during the first 13 ns and then it is stabilized to the *anti* one for the rest of the simulation time (Fig. 9B). Thus, the molecular dynamics approach points to the *anti* conformation as being most favorable in the micellar environment. Regarding the unhindered flunctuation of τ_2 around 90° as observed in the conformational analysis, this is also evident in the micellar environment (Supplementary material, Fig. S6). The mean values of the interatomic distances during the simulation time for both initial conformations of losartan (Table 2) were found to be very similar with the NMR derived values.

3.2.3. Interactions of losartan with AT_1 receptor embedded in a bilayer environment

MD simulations of losartan in a DPPC lipid bilayer with the AT_1 receptor embedded were also performed in order to study: a) the conformational dynamics of losartan in a lipid bilayer and at the vicinal region of AT_1 receptor; b) the positioning of losartan in the bilayer; and c) the diffusion pathway of losartan in the bilayer.

Losartan molecules were initially placed randomly in the water and lipid bilayer phases at a minimum distance of 20 Å from the AT1 receptor. It is evident from the simulations that losartan shows a strong

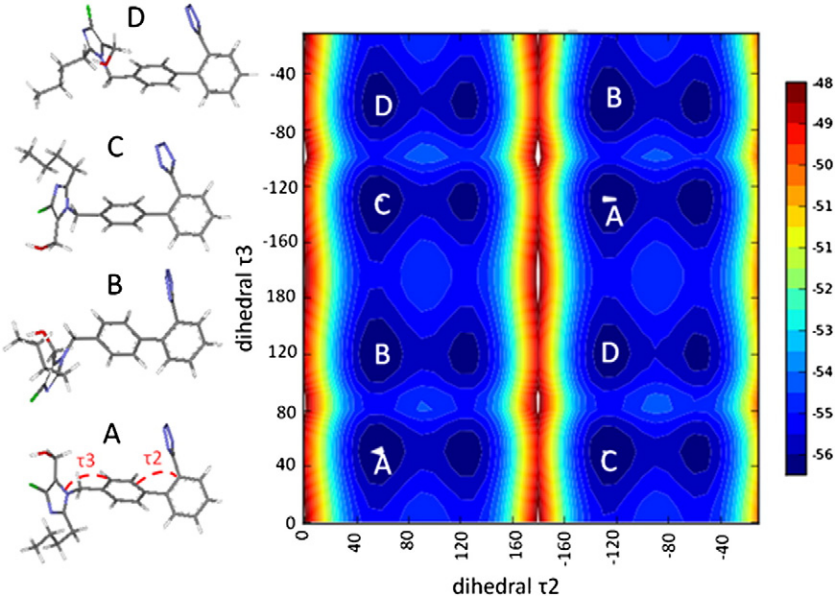

Fig. 6. Heat map illustrating the energy landscape (in kcal mol^{-1}) resulting from the grid scan search by varying the dihedrals τ_2 and τ_3. Low energy conformers are depicted. As a general rule, the *anti* conformers bear the torsions τ_2 and τ_3 with the same sign, while the *syn* conformers adopt opposite sign for those angles.

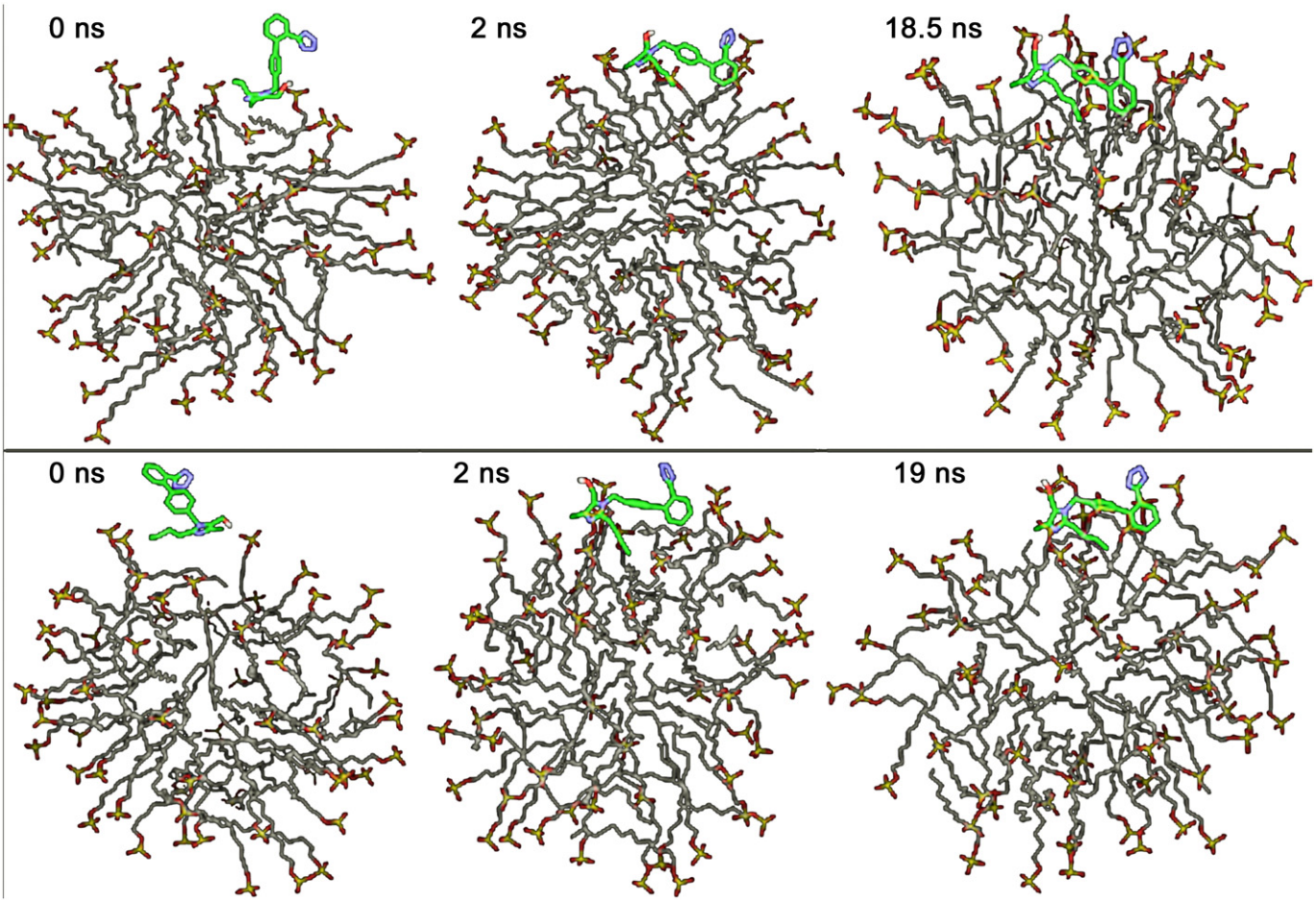

Fig. 7. Three snapshots of losartan (*anti* conformer, top) and (*syn* conformer, bottom) with the SDS micelle MD trajectory. At the beginning of the simulation time (0 ns) the drug lies in the aqueous environment outside of the micelle, after 2 ns it has approached the micelle surface, and then it is immersed within the micelle and practically localizes between the sulfate groups and the upper part of the dodecyl chains.

preference for the membrane environment with respect to the water phase, which is not surprising given the significant hydrophobic component of the drug solvent-accessible surface area [31]. Within the first few ns all losartan molecules partition spontaneously in the DPPC bilayer from the water phase with the exception of one molecule, which interacts with the extracellular part of the AT1 receptor. Likewise, all losartan molecules initially placed within the lipid bilayer remain there for the rest of the simulation time (Fig. 10). Losartan molecules diffuse freely along the membrane plane remaining close to lipid head groups and the water:bilayer interface (see Supporting video).

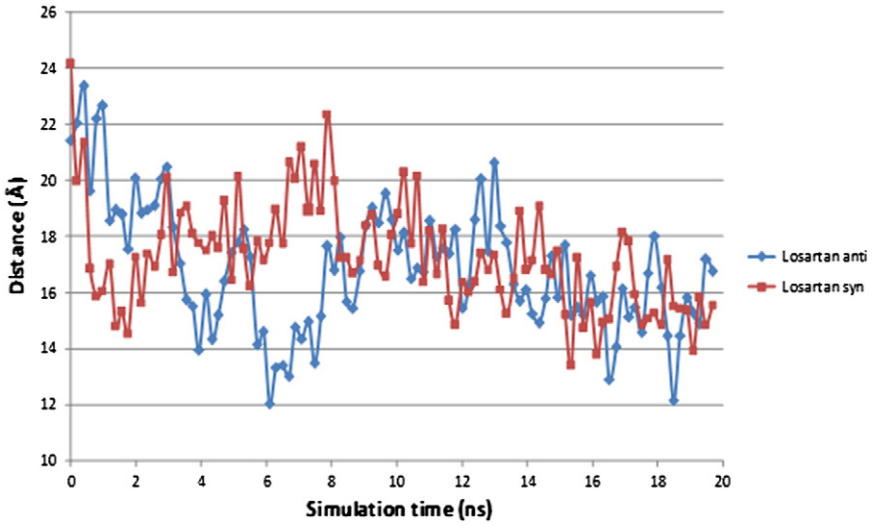

Fig. 8. Plot of the distance between the center of masses of losartan (*anti* in blue, *syn* in red) and of micelle throughout the simulation time.

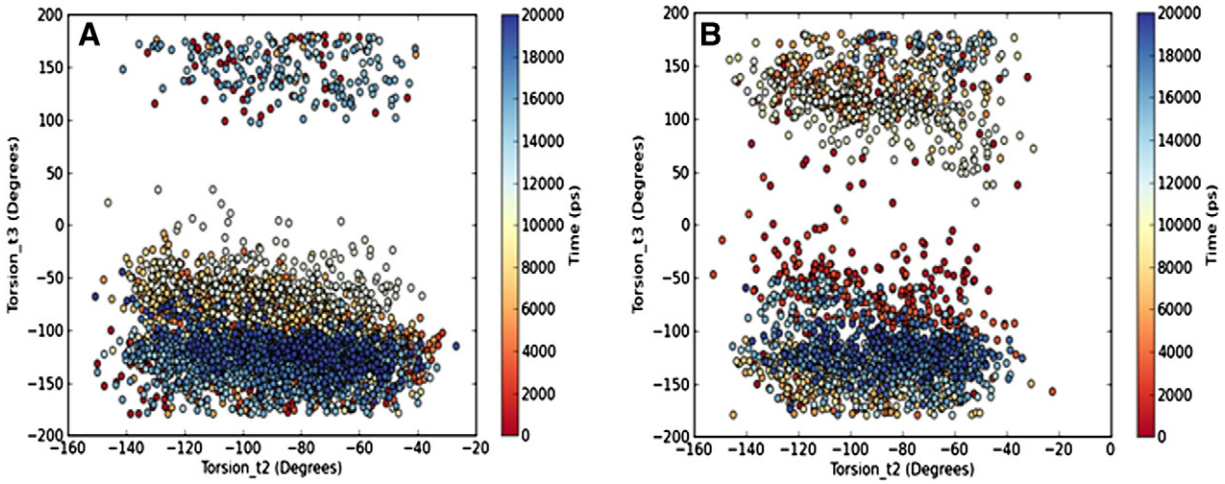

Fig. 9. Heat maps depicting the distribution of losartan torsion angles τ_2 and τ_3 throughout the simulation time in SDS micelles for the *anti* (A) and the *syn* (B) initial conformers. The *anti* conformation is characterized by values of τ_2 and τ_3 bearing the same sign while the *syn* conformation by values of τ_2 and τ_3 of opposite signs.

3.2.3.1. Drug–membrane interactions and positioning of losartan. In all cases, losartan positioned itself with the imidazole ring pointing toward the bilayer interface and the hydrophobic side chain embedded in the bilayer. Hydrogen bond analysis confirmed that losartan molecules interact predominantly with the lipid glycerol backbone and headgroup forming, on average, 0.35 hydrogen bonds per molecule with the carbonyl and ether oxygen atoms (total for all losartan molecules: 2.5 ± 1.4) and 0.35 hydrogen bonds per molecule with the phosphate group of the DPPC headgroup (total for all losartan molecules: 2.4 ± 1.4) (Supplementary material, Fig. S7a and d, respectively). The main contribution to hydrogen bonding of all losartan molecules with the DPPC glycerol backbone arises from the tetrazole moieties (1.8 ± 1.1), while the hydrogen bonds of the losartan hydroxymethyl groups to the glycerol backbone are limited to 0.6 ± 0.7 (Supplementary material, Fig. S7b and c, respectively). These hydrogen bond contributions are reversed for the interactions of losartan with the DPPC headgroup. In this case, the main contribution to hydrogen bonding of losartan with the phosphate group of DPPC arises from the losartan hydroxymethyl groups (2.4 ± 1.4 hydrogen bonds in total) relatively to the minor contribution of the tetrazole moieties, which form only 0.6 ± 0.7 hydrogen bonds (Supplementary material, Fig. S7f and e, respectively). The imidazole group did not form any hydrogen bonds with the DPPC headgroup throughout the course of the simulation. These data indicate a positioning of losartan consistent with the hydroxymethyl group pointing toward the DPPC headgroup, while the tetrazole moiety is oriented toward the DPPC glycerol backbone. Interestingly, despite the fact that all but one losartan molecules remain in the membrane throughout the simulation, they do form hydrogen bonds with water molecules that are close to or have penetrated the lipid bilayer yielding an average number of 1.6 hydrogen bonds for each molecule (total for all losartan molecules 11.6 ± 3.4). The tetrazole and hydroxymethyl moieties form on average one hydrogen bond with water in each molecule (Supplementary material, Fig. S7g–i). The imidazole moiety is buried under the hydroxymethyl group and positioned around the area of the glycerol backbone without forming any hydrogen bonds with the DPPC headgroup. However, it exhibits occasionally polar interactions with water at an average of 0.2 hydrogen bonds per molecule (Supplementary material, Fig. S7j). It should be also noted that losartan engages into infrequent intramolecular hydrogen bonding between its hydroxyl and tetrazole groups.

3.2.3.1.1. Intermolecular interactions — Solvation of losartan by DPPC molecules in the bilayer. To further investigate the intermolecular interactions of losartan with the lipid bilayer, radial pair distribution functions, $g(r)$, for several types of interactions were calculated. The $g(r)$ were estimated here from the equation

$$g(r) = \frac{V}{N}\left\langle \frac{n(r)}{4\pi r^2 dr} \right\rangle$$

where V is the volume of the simulation box containing N particles, and $n(r)$ is the number of particles y in the sphere of radius r and width dr around particle x. The first and second solvation shell occupancies may be calculated from the respective $g(r)$ functions by integrating up to the first and second minima, respectively (Table 3).

The solvation of the losartan hydroxyl by the DPPC glycerol backbone and headgroups, as calculated by the radial pair distribution function, is shown in Fig. 11a,b. A small sharp peak at 2 Å and a larger pronounced peak at 4 Å indicate that losartan hydroxyls are strongly solvated by the DPPC glycerol backbone and headgroup area and have on average two DPPC glycerol backbones and two DPPC headgroup neighbors at 4 Å (Table 3). The losartan tetrazole also shows a small sharp peak at 2 Å followed by another pronounced peak at 4 Å in the radial distribution function with the glycerol backbone (Fig. 11c). Integration up to the second minima shows that it has on average two glycerol backbone neighbors (Table 3). The losartan tetrazole interacts more strongly with the DPPC glycerol backbone rather than the DPPC headgroup as it has one DPPC headgroup neighbor at 5 Å (Fig. 11d and Table 3). Finally, the losartan butyl chain radial pair distribution function (Fig. 11e) shows that the first solvation shell of the butyl chain from the DPPC headgroup is found at ~12 Å, which is consistent with the observation that the butyl chain is buried in the bilayer hydrophobic core. These results confirm that losartan displays a strong preference to reside in the interface and interior of the lipid bilayer. This behavior may favor the assumption that losartan approaches the AT_1 receptor through an intermediate partitioning with the membrane rather than in a direct fashion.

3.2.3.2. Conformational dynamics of losartan. Losartan adopts a vertical orientation for the tetrazole ring with respect to the adjacent aromatic ring as seen from the distribution of dihedral angle τ_2 (Supplementary material, Fig. S8a) which shows a peak exactly at 90° as was also found in the SDS micelle simulation. No other peaks are observed for τ_2 indicating that the molecule "locks" itself in this position with a barrier of 8 kcal/mol (Supplementary material, Fig. S8b), in agreement with the results of the conformational analysis of losartan and our previously published studies [7]. We observe that losartan interconverts

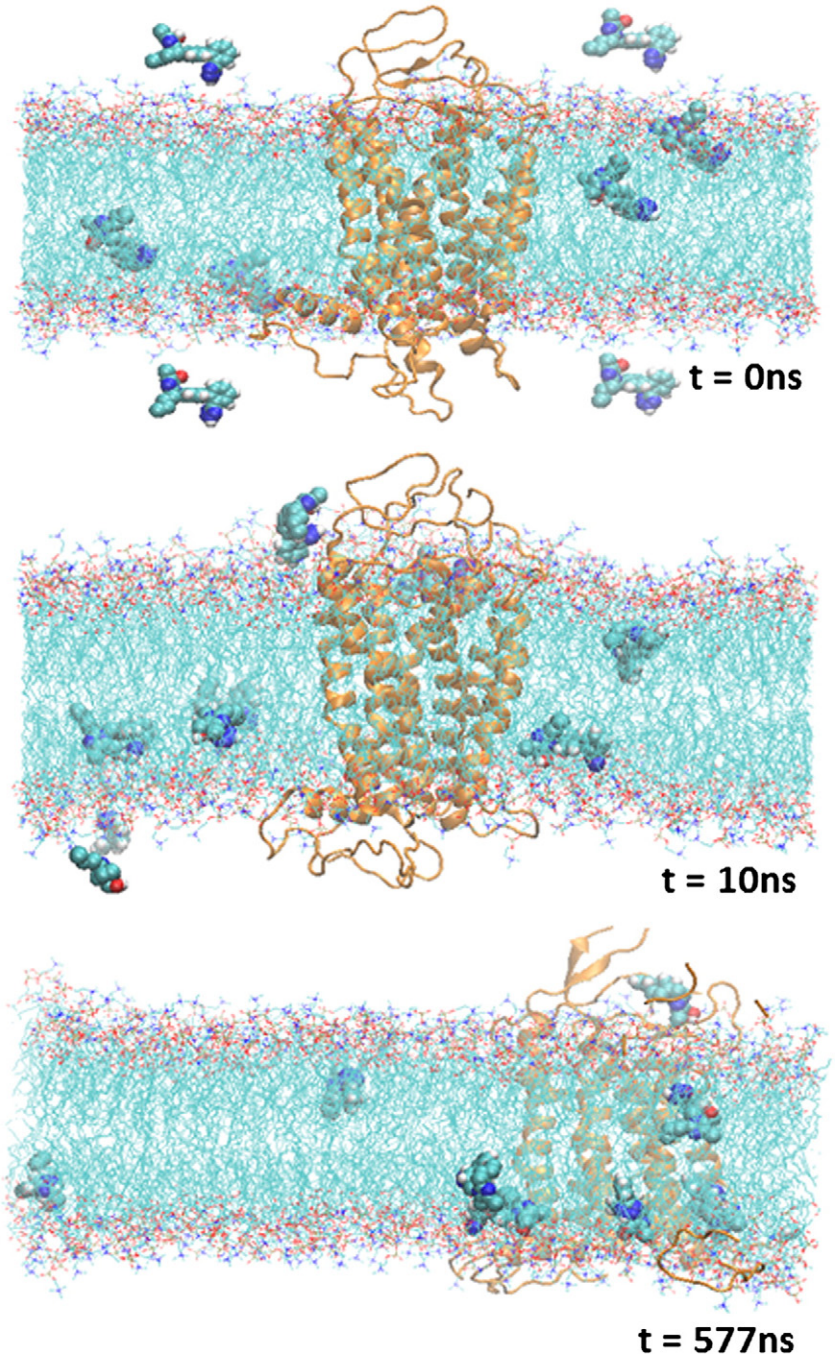

Fig. 10. Three snapshots of losartan in a DPPC lipid bilayer with the AT_1 receptor embedded MD trajectory. Losartan molecules were initially placed randomly in the water and lipid bilayer phases (t = 0 ns). Within the first 10 ns all but one losartan molecules partition spontaneously in the DPPC bilayer from the water phase. One molecule interacts with the extracellular part of the AT_1 receptor. During the rest of the simulation time, losartan molecules diffuse freely along the membrane plane remaining close to lipid headgroups.

Table 3
First and second average solvation shells for various groups in the simulation.

g(r)[a]	DPPC-losartan	
	First shell	Second shell
Losartan hydroxyl – DPPC glycerol backbone	0	2
Losartan hydroxyl – DPPC headgroup	0.1	2
Losartan tetrazole – DPPC glycerol backbone	0.1	2
Losartan tetrazole – DPPC headgroup	0	1

[a] The first solvation shell was calculated by integrating the corresponding pair radial distribution function up to the first minimum.

dynamically between the *anti* (τ_3 varying around +100°) and the *syn* (τ_3 varying around −100°) conformations (Supplementary material, Fig. S8c) with a barrier of ~2 kcal/mol (Supplementary material, Fig. S8d) as also estimated from the systematic scan around the dihedrals τ_2 and τ_3 (Fig. 6). This dynamic behavior is also mapped in Fig. S9 of the Supplementary material, where a marginal predominance of the *anti* conformation is observed after 400 ns of the simulation time (half of the molecules prefer the *anti* conformation at an average percentage of 67%), while it seems to prevail after 500 ns since 6 out of 8 molecules adopt the *anti* conformation at an average percentage of 76%.

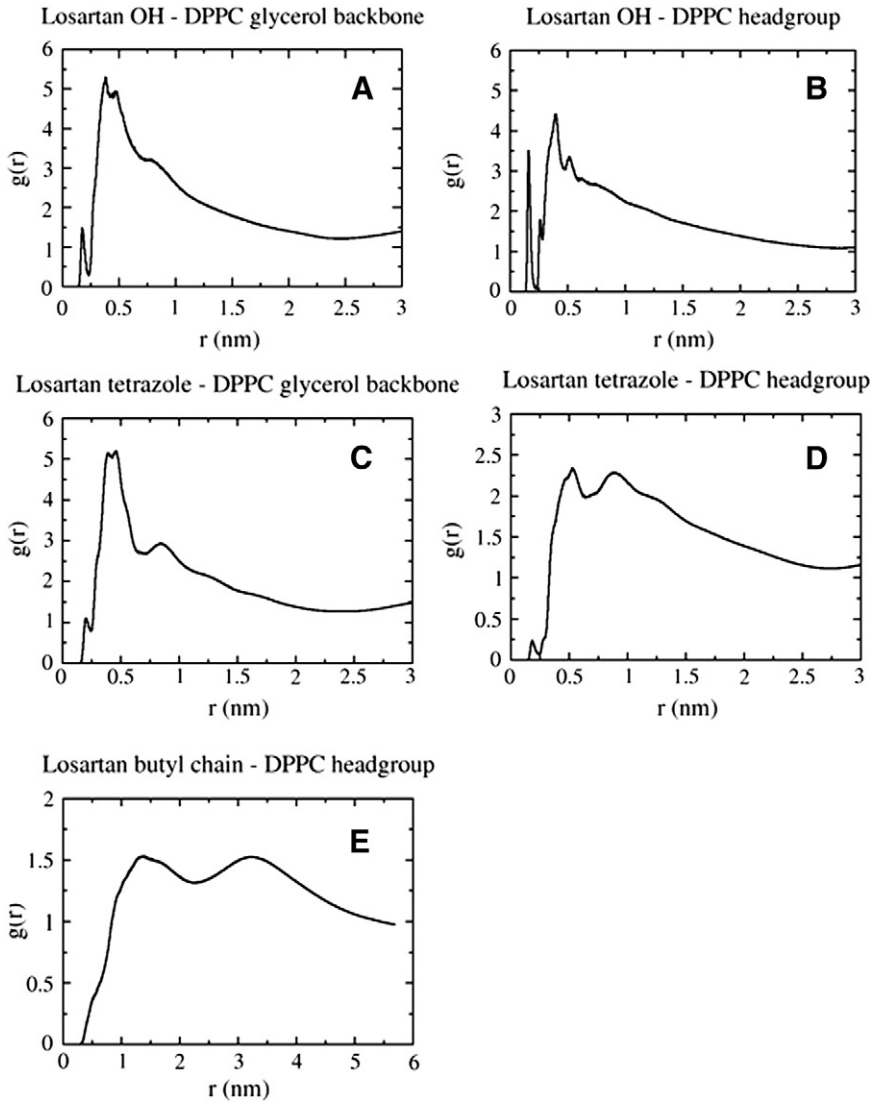

Fig. 11. Radial pair distribution functions of losartan (a) hydroxyl relative to DPPC glycerol backbone, (b) hydroxyl relative to DPPC headgroup, (c) tetrazole relative to DPPC glycerol backbone, (d) tetrazole relative to DPPC headgroup, and (e) butyl chain relative to DPPC headgroup. Results are averaged over all losartan molecules, which are embedded in the bilayer.

3.2.3.3. Calculation of interatomic distances. The interatomic distances, derived from the NMR data, were also calculated from the MD trajectories of the simulations in the membrane environment. The results are in good agreement with the NMR measured values indicating the validity of our approach (Table 2).

3.2.3.4. Diffusion of losartan in the bilayer. The diffusion of losartan within the lipid bilayer embedding the AT_1 receptor was calculated from the linear regime (100–400 ns) of the mean square displacement of the molecules (Supplementary material, Fig. S10). The lateral diffusion coefficient is $D = 3.02 \pm 1 \times 10^{-11}$ m^2 s^{-1}, which is in excellent agreement with the experimentally derived diffusion constant from DOSY NMR experiments in the micellar environment ($D = 4.3 \pm 0.4 \times 10^{-11}$ m^2 s^{-1}), indicating that micelle aggregates can simulate in a very efficient way the membrane environment.

3.2.3.5. Diffusion of losartan toward the AT_1 receptor. Only one losartan molecule was found to encounter the receptor from the water phase by interacting with the extracellular loops throughout the ~600 ns of the MD trajectory. The rest are found to diffuse freely within the bilayer though without approaching the receptor. Various reasons may be formulated justifying the inability of the drug to reach the active site in this time scale either from the extracellular surface or through the bilayer core.

(i) *Obstacles reaching the active site through direct action on the receptor*. The homology model of AT_1 used in the present study was constructed using the bovine rhodopsin structure as a template, where the extracellular loop 2 sits above the binding site and encloses it. As already mentioned in the introduction, a recently published model of AT1 based on the chemokine CXCR4 receptor [21,22], is characterized by an open ECL2 loop, presumably enabling easier doping of losartan; this issue will be further investigated in future studies using the newer homology model available. Therefore, the rearrangements needed for our model to adopt the open state of the extracellular loop 2 may occur in the ms time scale, whereas the time scale reachable by the current state-of-the-art all-atom MD simulations is in the order of μs. Moreover, different experimental MD conditions may have to be used (i.e. higher temperature) in order to increase the flexibility of the ligand and receptor and thus avoid the trapping.

ii) *Obstacles reaching the active site through bilayer diffusion*. The complexity of the membrane in a realistic system (containing cholesterol, rigid ion channels, etc.) hinders the diffusion of the AT_1 receptor compared to our model, where the receptor may freely diffuse in the plane of a pure DPPC bilayer. This higher mobility of the AT_1 receptor may not favor the encounter with the drug molecules. Lastly, the diffusion of losartan toward the active site of the AT_1 receptor may be retarded by its stronger binding to the headgroup and upper lipophilic segment of the lipid bilayers.

In conclusion, the presented results were based on a simplified membrane bilayer:receptor model of the much more complicated system of natural membranes. Other factors influencing the partitioning of the drug in the membrane could involve the induction of the interdigitation effect by the drug, the presence of cholesterol, which has been shown to compete with drug incorporation in the membrane, or the presence of domains with high percentage of not well-packed phospholipids such as dioleoylphosphatidylcholine, which facilitate drug diffusion [60].

4. Conclusions

This study investigates the conformational features of losartan in different environments simulating biological fluids and membrane bilayers. Moreover, in an effort to investigate the hypothesis of spontaneous insertion and partitioning of losartan in the membrane bilayer followed by lateral diffusion towards the AT1 TM receptor we have applied an integrated methodology consisting of NMR experiments and MD simulations approaches.

The drug can adopt two major conformations in solution positioning the tetrazole and imidazole moieties in an *anti* or a *syn* orientation with respect to the A phenyl ring plane. MD simulations in implicit solvation models driven by NOE interatomic distances support the interconversion between the *anti* and *syn* conformations, which are allowed by the energetically favorable rotation around the critical torsion angle τ_3, which bridges the biphenyl tetrazole with imidazole.

Evidence for self-assembly behavior was observed in aqueous solution at the highest studied concentration, which is possibly associated with the charged tetrazole moiety of the drug and the presence of K^+ counterions. Self-association of losartan at high concentrations in DPPC bilayers has also been reported, resulting in the formation of drug-rich and drug-poor domains and possibly retarding its diffusion towards the AT_1 receptor [14,31].

The drug topography in lipid environment was studied by NMR relaxation probes and drug:micelle intermolecular ROE interactions, which located losartan near the micellar surface. The hydroxymethyl moiety and the tetrazole face the micelle–water interface, while the butyl chain is positioned towards the micellar core. This topography is also supported by MD simulations of losartan loaded in SDS as well as in the membrane mimicking DPPC bilayer environment.

The spontaneous insertion of losartan in the lipidic core was confirmed by MD simulations in both micellar and lipid bilayers with the AT_1 receptor embedded. The drug approaches the lipid surface from the aqueous environment within the first few ns, swifts into the bilayer and diffuses between the polar headgroups and the upper part of the alkyl chains of the lipids. In accordance with the proposed localisation of losartan, the long exploratory MD simulation run in the DPPC lipid bilayer revealed the formation of hydrogen bonds with the lipid glycerol backbone and the phosphate groups as well as isolated water molecules penetrating the lipid bilayer. As a general trend, the *anti* conformation of losartan seems to be the most favorable in both the SDS and DPPC environments pointing to this conformer as the bioactive one in a membrane environment.

The calculated interatomic distances in both membrane-mimicking environments were in excellent agreement with the experimental distances measured by NMR. It is also noteworthy, that the calculated lateral diffusion coefficient in the lipid bilayer is perfectly in line with the measured one from DOSY NMR spectroscopy in the micellar environment. Our integrated approach is thus validated by the convergence of the experimental and the theoretical data.

Overall, *in silico* and NMR approaches support the assumption that the membrane environment serves as a pool of drug molecules locally trapped and potentially diffusing towards the embedded AT_1 receptor active site. This localisation restricts the drug flexibility and probably contributes to the effective interaction with the receptor while it could additional probe alternative pathways of entrance towards the AT1 active site beyond the random encounter at the extracellular part.

Furthermore, it has been reported that the free drug molecules with high membrane affinity could be “trapped” inside the membrane bilayer and consecutively bind to the same target and/or targets nearby, even when their concentration in the bulk aqueous phase has already dropped to insignificant levels [61]. In this respect, monitoring drug interaction with membranes can provide valuable information for designing new long acting drugs.

The aqueous-membrane “walk” of losartan at atomic resolution was implemented as a continuation to our previous studies [11,31,62,63] on the interactions of the amphiphiles AT_1 antagonists with membranes and the possible implication of the latter in the effective interaction of the drug with its target. Moreover, there is increasing evidence referring to the beneficial anti-inflammatory and neuroprotective efficacy of sartans either directly by blockade of the brain AT_1 receptors or indirectly by inhibiting further inflammatory cascades or maintaining the functionality of the blood–brain barrier (BBB) during inflammation. A number of studies have evaluated their effects with systemic administration thus probing to their ability to cross the BBB [64]. Their distinct pharmacological profile could also be related with the different degree of sartans' permeability of the BBB. The effort to understand their interactions with membranes might prove to be useful for gaining insights of the sartan transportation mechanism in the human tissues, and also for designing novel drugs with improved therapeutic profile.

Supplementary data and supporting video to this article can be found online at http://dx.doi.org/10.1016/j.bbamem.2013.12.012.

Acknowledgement

Funding was granted by European Union's Seventh Framework Programme (FP7-REGPOT-2009-1) under grant agreement no. 245866 (to CP). The authors acknowledge LANCOM Ltd for providing cloud services.

References

[1] S.Y. Yang, Pharmacophore modeling and applications in drug discovery: challenges and recent advances, Drug Discov. Today 15 (2010) 444–450.
[2] H. Kubinyi, Success stories of computer-aided design, in: S. Ekins (Ed.), Computer Applications in Pharmaceutical Research and Development, John Wiley & Sons, Inc., Hoboken, NJ, USA, 2006.
[3] T. Mavromoustakos, M. Zervou, P. Zoumpoulakis, I. Kyrikou, N.P. Benetis, L. Polevaya, P. Roumelioti, N. Giatas, A. Zoga, P.M. Minakakis, A. Kolocouris, D. Vlahakos, S.G. Grdadolnik, J. Matsoukas, Conformation and bioactivity. Design and discovery of novel antihypertensive drugs, Curr. Top. Med. Chem. 4 (2004) 385–401.
[4] B. Musafia, H. Senderowitz, Biasing conformational ensembles towards bioactive-like conformers for ligand-based drug design, Expert Opin. Drug Discovery 5 (2010) 943–959.
[5] R.R. Wexler, W.J. Greenlee, J.D. Irvin, M.R. Goldberg, K. Prendergast, R.D. Smith, P.B.M.W.M. Timmermans, Nonpeptide angiotensin II receptor antagonists: the next generation in antihypertensive therapy, J. Med. Chem. 39 (1996) 625–656.
[6] K. Dickstein, P. Timmermans, R. Segal, Losartan: a selective angiotensin II type 1 (AT1) receptor antagonist for the treatment of heart failure, Expert Opin. Investig. Drugs 7 (1998) 1897–1914.
[7] T. Mavromoustakos, A. Kolocouris, M. Zervou, P. Roumelioti, J. Matsoukas, R. Weisemann, An effort to understand the molecular basis of hypertension through the study of conformational analysis of Losartan and Sarmesin using a combination of nuclear magnetic resonance spectroscopy and theoretical calculations, J. Med. Chem. 42 (1999) 1714–1722.

[8] X.R. Hu, Y.W. Wang, J.M. Gu, Losartan potassium 3.5-hydrate, a new crystalline form, Acta Crystallogr. E 61 (2005) M1686–M1688.
[9] D. Fernandez, D. Vega, J.A. Ellena, G. Echeverria, Losartan potassium, a non-peptide agent for the treatment of arterial hypertension, Acta Crystallogr. C 58 (2002) m418–m420.
[10] L. Tessler, I. Goldberg, Losartan, an antihypertensive drug, Acta Crystallogr. E 60 (2004) o1830–o1832.
[11] P. Zoumpoulakis, I. Daliani, M. Zervou, I. Kyrikou, E. Siapi, G. Lamprinidis, E. Mikros, T. Mavromoustakos, Losartan's molecular basis of interaction with membranes and AT1 receptor, Chem. Phys. Lipids 125 (2003) 13–25.
[12] C. Fotakis, D. Christodouleas, P. Chatzigeorgiou, M. Zervou, N.P. Benetis, K. Viras, T. Mavromoustakos, Development of a CP ^{31}P NMR broadline simulation methodology for studying the interactions of antihypertensive AT1 antagonist losartan with phospholipid bilayers, Biophys. J. 96 (2009) 2227–2236.
[13] T. Mavromoustakos, S. Durdagi, C. Koukoulitsa, M. Simcic, M.G. Papadopoulos, M. Hodoscek, S.G. Grdadolnik, Strategies in the rational drug design, Curr. Med. Chem. 18 (2011) 2517–2530.
[14] E. Theodoropoulou, D. Marsh, Interactions of angiotensin II non-peptide AT(1) antagonist losartan with phospholipid membranes studied by combined use of differential scanning calorimetry and electron spin resonance spectroscopy, Biochim. Biophys. Acta 1461 (1999) 135–146.
[15] M.A. Bhuiyan, M. Ishiguro, M. Hossain, T. Nakamura, M. Ozaki, S. Miura, T. Nagatomo, Binding sites of valsartan, candesartan and losartan with angiotensin II receptor 1 subtype by molecular modeling, Life Sci. 85 (2009) 136–140.
[16] T. Tuccinardi, V. Calderone, S. Rapposelli, A. Martinelli, Proposal of a new binding orientation for non-peptide AT1 antagonists: homology modeling, docking and three-dimensional quantitative structure–activity relationship analysis, J. Med. Chem. 49 (2006) 4305–4316.
[17] C. Baleanu-Gogonea, S. Karnik, Model of the whole rat AT1 receptor and the ligand-binding site, J. Mol. Model. 12 (2006) 325–337.
[18] H. Unal, R. Jagannathan, A. Bhatnagar, K. Tirupula, R. Desnoyer, S.S. Karnik, Long range effect of mutations on specific conformational changes in the extracellular loop 2 of angiotensin II type 1 receptor, J. Biol. Chem. 288 (2013) 540–551.
[19] S. Topiol, M. Sabio, X-ray structure breakthroughs in the GPCR transmembrane region, Biochem. Pharmacol. 78 (2009) 11–20.
[20] M. Congreve, C.J. Langmead, J.S. Mason, F.H. Marshall, Progress in structure based drug design for G protein-coupled receptors, J. Med. Chem. 54 (2011) 4283–4311.
[21] M.T. Matsoukas, C. Potamitis, P. Plotas, M.E. Androutsou, G. Agelis, J. Matsoukas, P. Zoumpoulakis, Insights into AT1 receptor activation through AngII binding studies, J. Chem. Inf. Model 53 (2013) 2798–2811.
[22] M.T. Matsoukas, A. Cordomi, S. Rios, L. Pardo, T. Tselios, Ligand binding determinants for Angiotensin II Type 1 receptor from computer simulations, J. Chem. Inf. Model 53 (2013) 2874–2883.
[23] S. Nagar, K. Korzekwa, Commentary: nonspecific protein binding versus membrane partitioning: it is not just semantics, Drug Metab. Dispos. 40 (2012) 1649–1652.
[24] G. Vauquelin, A. Packeu, Ligands, their receptors and … plasma membranes, Mol. Cell. Endocrinol. 311 (2009) 1–10.
[25] A.M. Seddon, D. Casey, R.V. Law, A. Gee, R.H. Templer, O. Ces, Drug interactions with lipid membranes, Chem. Soc. Rev. 38 (2009) 2509–2519.
[26] Y. Xu, V.E. Yushmanov, P. Tang, NMR studies of drug interaction with membranes and membrane-associated proteins, Biosci. Rep. 22 (2002) 175–196.
[27] D.E. Warschawski, A.A. Arnold, M. Beaugrand, A. Gravel, E. Chartrand, I. Marcotte, Choosing membrane mimetics for NMR structural studies of transmembrane proteins, Biochim. Biophys. Acta 1808 (2011) 1957–1974.
[28] D.L. Daleke, Regulation of transbilayer plasma membrane phospholipid asymmetry, J. Lipid Res. 44 (2003) 233–242.
[29] T.R. Oliveira, M.T. Lamy, U.M. De Paula, L.L. Guimaraes, M.S. Toledo, H.K. Takahashi, A.H. Straus, C.J. Lindsey, T.B. Paiva, Structural properties of lipid reconstructs and lipid composition of normotensive and hypertensive rat vascular smooth muscle cell membranes, Braz. J. Med. Biol. Res. 42 (2009) 844–885.
[30] P. Sokkar, S. Mohandass, M. Ramachandran, Multiple templates-based homology modeling enhances structure quality of AT1 receptor: validation by molecular dynamics and antagonist docking, J. Mol. Model. 17 (2011) 1565–1577.
[31] C. Fotakis, D. Christodouleas, P. Zoumpoulakis, E. Kritsi, N.P. Benetis, T. Mavromoustakos, H. Reis, A. Gili, M.G. Papadopoulos, M. Zervou, Comparative biophysical studies of sartan class drug molecules losartan and candesartan (CV-11974) with membrane bilayers, J. Phys. Chem. B 115 (2011) 6180–6192.
[32] F. Li, L. Wang, N. Xiao, M. Yang, L. Jiang, M. Liu, Dominant conformation of valsartan in sodium dodecyl sulfate micelle environment, J. Phys. Chem. B 114 (2010) 2719–2727.
[33] C. Cao, J. Mao, F. Li, M. Yang, H. He, L. Jiang, M. Liu, Understanding the interaction between valsartan and detergents by NMR techniques and molecular dynamics simulation, J. Phys. Chem. B 116 (2012) 7470–7478.
[34] A.D. Mackerell, Molecular-dynamics simulation analysis of a sodium dodecyl-sulfate micelle in aqueous-solution — Decreased fluidity of the micelle hydrocarbon interior, J. Phys. Chem. 99 (1995) 1846–1855.
[35] http://moose.bio.ucalgary.ca/index.php?page=Structures_and_Topologies(Access date: 18/11/2013).
[36] C. Fotakis, S. Gega, E. Siapi, C. Potamitis, K. Viras, P. Moutevelis-Minakakis, C.G. Kokotos, S. Durdagi, S.G. Grdadolnik, B. Sartori, M. Rappolt, T. Mavromoustakos, Interactions at the bilayer interface and receptor site induced by the novel synthetic pyrrolidinone analog MMK3, BBA-Biomembr. 1798 (2010) 422–432.
[37] M. Lindberg, J. Jarvet, U. Langel, A. Graslund, Secondary structure and position of the cell-penetrating peptide transportan in SDS micelles as determined by NMR, Biochemistry 40 (2001) 3141–3149.
[38] S.G. Grdadolnik, D.F. Mierke, Vancomycin: interactions with a model cell membrane, Biopolymers 42 (1997) 627–632.
[39] C. Griesinger, R.R. Ernst, Frequency offset effects and their elimination in NMR rotating-frame cross-relaxation spectroscopy, J. Magn. Reson. 75 (1987) 261–271.
[40] MacroModel, version 9.9, Schrödinger, LLC, New York, NY, 2012.
[41] A. Chaudhuri, S. Haldar, A. Chattopadhyay, Organization and dynamics in micellar structural transition monitored by pyrene fluorescence, Biochem. Biophys. Res. Commun. 390 (2009) 728–732.
[42] E.L. Doyle, C.A. Hunter, H.C. Phillips, S.J. Webb, N.H. Williams, Cooperative binding at lipid bilayer membrane surfaces, J. Am. Chem. Soc. 125 (2003) 4593–4599.
[43] Desmond Molecular Dynamics System, version 3.1, D. E. Shaw Research, New York, NY, 2012. (Maestro-Desmond Interoperability Tools, version 3.1, Schrödinger, New York, NY, 2012).
[44] M. Tuckerman, B.J. Berne, G.J. Martyna, Reversible multiple time scale molecular-dynamics, J. Chem. Phys. 97 (1992) 1990–2001.
[45] H.J.C. Berendsen, J.P.M. Postma, W.F. Vangunsteren, A. Dinola, J.R. Haak, Molecular-dynamics with coupling to an external bath, J. Chem. Phys. 81 (1984) 3684–3690.
[46] U. Essmann, L. Perera, M.L. Berkowitz, T. Darden, H. Lee, L.G. Pedersen, A smooth particle mesh Ewald method, J. Chem. Phys. 103 (1995) 8577–8593.
[47] Maestro, version 9.3, Schrödinger, LLC, New York, NY, 2012.
[48] The PyMOL Molecular Graphics System, Version 1.5.0.4 Schrödinger, LLC.
[49] H.J.C. Berendsen, D. van der Spoel, R. van Drunen, GROMACS: a message-passing parallel molecular dynamics implementation, Comput. Phys. Commun. 91 (1995) 43–56.
[50] C. Oostenbrink, A. Villa, A.E. Mark, W.F. van Gunsteren, A biomolecular force field based on the free enthalpy of hydration and solvation: the GROMOS force-field parameter sets 53A5 and 53A6, J. Comput. Chem. 25 (2004) 1656–1676.
[51] J.F. Nagle, R.T. Zhang, S. TristramNagle, W.J. Sun, H.I. Petrache, R.M. Suter, X-ray structure determination of fully hydrated L(alpha) phase dipalmitoylphosphatidylcholine bilayers, Biophys. J. 70 (1996) 1419–1431.
[52] M.G. Wolf, M. Hoefling, C. Aponte-Santamaria, H. Grubmuller, G. Groenhof, g_membed: efficient insertion of a membrane protein into an equilibrated lipid bilayer with minimal perturbation, J. Comput. Chem. 31 (2010) 2169–2174.
[53] http://davapc1.bioch.dundee.ac.uk/cgi-bin/prodrg/(Access date: 18/11/2013).
[54] J.A. Lemkul, W.J. Allen, D.R. Bevan, Practical considerations for building GROMOS-compatible small-molecule topologies, J. Chem. Inf. Model. 50 (2010) 2221–2235.
[55] M. Valiev, E.J. Bylaska, N. Govind, K. Kowalski, T.P. Straatsma, H.J.J. van Dam, D. Wang, J. Nieplocha, E. Apra, T.L. Windus, W.A. de Jong, NWChem: a comprehensive and scalable open-source solution for large scale molecular simulations, Comput. Phys. Commun. 181 (2010).
[56] http://www.nwchem-sw.org/(Access date: 18/11/2013).
[57] J. Rebek Jr., Contortions of encapsulated alkyl groups, Chem. Commun. (2007) 2777–2789.
[58] R. Vijay, A.B. Mandal, G. Baskar, ^{1}H NMR spectroscopic investigations on the conformation of amphiphilic aromatic amino acid derivatives in solution: effect of chemical architecture of amphiphiles and polarity of solvent medium, J. Phys. Chem. B 114 (2010) 13691–13702.
[59] H.W. Van Den Hooven, C.A. Spronk, M. Van De Kamp, R.N. Konings, C.W. Hilbers, F.J. Van De Van, Surface location and orientation of the lantibiotic nisin bound to membrane-mimicking micelles of dodecylphosphocholine and of sodium dodecylsulphate, Eur. J. Biochem. 235 (1996) 394–403.
[60] A. Hodzic, P. Zoumpoulakis, G. Pabst, T. Mavromoustakos, M. Rappolt, Losartan's affinity to fluid bilayers modulates lipid–cholesterol interactions, Phys. Chem. Chem. Phys. 14 (2012) 4780–4788.
[61] G. Vauquelin, S.J. Charlton, Long-lasting target binding and rebinding as mechanisms to prolong in vivo drug action, Br. J. Pharmacol. 161 (2010) 488–508.
[62] C. Fotakis, G. Megariotis, D. Christodouleas, E. Kritsi, P. Zoumpoulakis, D. Ntountaniotis, M. Zervou, C. Potamitis, A. Hodzic, G. Pabst, M. Rappolt, G. Mali, J. Baldus, C. Glaubitz, M.G. Papadopoulos, A. Afantitis, G. Melagraki, T. Mavromoustakos, Comparative study of the AT(1) receptor prodrug antagonist candesartan cilexetil with other sartans on the interactions with membrane bilayers, Biochim. Biophys. Acta 1818 (2012) 3107–3120.
[63] C. Potamitis, M. Zervou, V. Katsiaras, P. Zoumpoulakis, S. Durdagi, M.G. Papadopoulos, J.M. Hayes, S.G. Grdadolnik, I. Kyrikou, D. Argyropoulos, G. Vatougia, T. Mavromoustakos, Antihypertensive drug valsartan in solution and at the AT(1) receptor: conformational analysis, dynamic NMR spectroscopy, Silico docking, and molecular dynamics simulations, J Chem Inf Model, 49, 2009, pp. 726–739.
[64] J.M. Saavedra, Angiotensin II AT(1) receptor blockers as treatments for inflammatory brain disorders, Clin. Sci. 123 (2012) 567–590.